

Streaming Sliced Optimal Transport

Khai Nguyen

The University of Texas at Austin

January 5, 2026

Abstract

Sliced optimal transport (SOT), or sliced Wasserstein (SW) distance, is widely recognized for its statistical and computational scalability. In this work, we further enhance computational scalability by proposing the first method for estimating SW from sample streams, called *streaming sliced Wasserstein* (Stream-SW). To define Stream-SW, we first introduce a streaming estimator of the one-dimensional Wasserstein distance (1DW). Since the 1DW has a closed-form expression, given by the absolute difference between the quantile functions of the compared distributions, we leverage quantile approximation techniques for sample streams to define a streaming 1DW estimator. By applying the streaming 1DW to all projections, we obtain Stream-SW. The key advantage of Stream-SW is its low memory complexity while providing theoretical guarantees on the approximation error. We demonstrate that Stream-SW achieves a more accurate approximation of SW than random subsampling, with lower memory consumption, when comparing Gaussian distributions and mixtures of Gaussians from streaming samples. Additionally, we conduct experiments on point cloud classification, point cloud gradient flows, and streaming change point detection to further highlight the favorable performance of the proposed Stream-SW¹.

1 Introduction

Optimal transport and the Wasserstein distance [43, 53] have led to numerous advancements in machine learning, statistics, and data science. For example, the Wasserstein distance has been used to enhance generative models such as generative adversarial networks (GANs) [3], autoencoders [50], and diffusion models via flow matching [29, 44, 51]. Additionally, it serves as a distortion (reconstruction) metric in point cloud applications [1], facilitates multimodal representation learning [31, 47], and aids in approximate Bayesian inference [4, 2, 49], among other applications.

Despite these benefits, the Wasserstein distance is computationally expensive. Specifically, its time complexity scales as $\mathcal{O}(n^3 \log n)$ [42], where n is the maximum number of support points across two distributions. Moreover, it suffers from the curse of dimensionality, with a sample complexity of order $\mathcal{O}(n^{-1/d})$ [18], where d is the number of dimensions. Consequently, in high-dimensional settings, a significantly larger number of samples is required to accurately approximate the distance between two unknown distributions using their empirical counterparts. This limitation makes the Wasserstein distance both statistically and computationally impractical in high dimensions.

Along with entropic regularization [13], which can reduce the time complexity of computing the Wasserstein distance to $\mathcal{O}(n^2)$ and overcome the curse of dimensionality, sliced optimal transport [36] (SOT) or the sliced Wasserstein (SW) distance [9] provides an alternative approach to mitigate computational challenges. SW is defined as the expectation of the one-dimensional Wasserstein (1DW) distance between random one-dimensional Radon projections [21] of two original distributions.

¹Code for this paper is published at <https://github.com/khainb/StreamSW>.

Since 1DW has a closed-form solution, given by the absolute difference between the quantile functions, SW achieves a time complexity of $\mathcal{O}(n \log n)$ and a memory complexity of $\mathcal{O}(n)$ when comparing discrete distributions with at most n supports. More importantly, SW distance does not suffer from the curse of dimensionality, with a sample complexity of $\mathcal{O}(n^{-1/2})$, making it both computationally and statistically scalable in any dimension. As a result, SW distance has been successfully applied in various domains, including generative models [15], domain adaptation [26], clustering [25], gradient flows [30, 7], Bayesian inference computation [34, 57], posterior summarization [39], two-sample testing [22], density-regression [12, 40], and more.

Streaming data is increasingly common in scientific and technological applications, especially with small devices such as Internet of Things (IoT) devices, which collect, process, and transmit large volumes of data in real time. These devices face challenges due to limited memory and computational power, requiring streaming algorithms that process each data point independently and efficiently, without storing large amounts of data. This drives the need for single-pass algorithms that use minimal memory. As distribution comparison is one of the most vital tasks in data science, computing the distance between two distributions from their sample streams becomes a natural and important challenge to address from theory to practice.

Recently, there has been growing interest in computing optimal transport, such as the Wasserstein distance, from streaming samples of two distributions. Online Sinkhorn [33] was the first algorithm to address entropic optimal transport in the streaming/online setting. However, Online Sinkhorn has a time complexity of $\mathcal{O}(n^2)$ and a memory complexity of $\mathcal{O}(n)$, as it requires storing all previously visited data. As a result, it remains impractical for streaming applications. Compressed Online Sinkhorn [54] attempts to mitigate this issue by employing measure compression. However, performing measure compression, such as Gaussian quadrature, is computationally expensive, exhibiting super-cubic complexity, which is undesirable in streaming settings with limited computational resources. Furthermore, the compression in Compressed Online Sinkhorn scales poorly with dimension, with a sample complexity of $\mathcal{O}(m^{-1/d})$, where m is the compressed support size. Consequently, the algorithm also remains computationally expensive. A natural question arises: “Could we adapt SOT and SW to the streaming setting?”

We provide the first answer to the question by proposing the first streaming version of the SW distance. To achieve this goal, we bridge the literature on *streaming quantile approximation* and *sliced optimal transport* by leveraging the previously discussed insight that the 1DW is computed based on quantile functions.

Contribution. In summary, our contributions are three-fold:

1. We first propose using quantile sketches as a data structure for estimating cumulative distribution functions (CDFs) and quantile functions of distributions from streaming samples. We then derive probabilistic bounds that characterize the approximation guarantees of these streaming estimators for both CDFs and quantile functions. Leveraging these results, we introduce the first streaming estimators of the one-dimensional Wasserstein (1DW) distance and the corresponding one-dimensional optimal transport map from sample streams. In addition, we establish probabilistic bounds for the approximation errors of the proposed streaming estimators for discussed quantities.
2. Using the streaming estimator of 1DW for one-dimensional projections, we introduce streaming Sliced Wasserstein (Stream-SW), the first streaming estimator for the SW distance. We then extend the probabilistic bounds for the approximation errors from 1DW to Stream-SW. Moreover, we discuss

how Stream-SW can be estimated using a finite number of projections and derive the corresponding guarantees for the proposed estimator. Furthermore, we analyze the computational complexity of Stream-SW, including both space and time complexities with respect to the number of streaming samples and the size of the quantile sketches. In summary, the space complexity of Stream-SW is logarithmic in the number of streaming samples and linear in the initial sketch size, while the time complexity is linear in the number of streaming samples and nearly linear in the initial sketch size.

3. Empirically, we demonstrate that Stream-SW achieves a more accurate approximation and offers better downstream performance compared to SW with random sampling (i.e., retaining only a random subset of streaming samples). Specifically, we first conduct simulations comparing Gaussians and Gaussian mixtures from sample streams. We then apply Stream-SW to streaming point-cloud classification using K-nearest neighbors, followed by a comparison in a streaming gradient flow setting. Finally, we showcase the effectiveness of Stream-SW in streaming change point detection using Kinect gesture dataset.

Organization. We begin by reviewing background on the Sliced Wasserstein distance in Section 2. Next, we discuss the definition of quantile sketch, propose streaming CDFs estimation, streaming quantile function estimation, streaming 1DW, Stream-SW, and their theoretical and computational properties in Section 3. Section 4 presents simulations and experiments. Finally, we conclude in Section 5. Additional materials, including technical proofs, detailed experiment descriptions, and supplementary experimental results, are provided in the Appendices.

Notations. For any $d \geq 2$, we define the unit hypersphere as $\mathbb{S}^{d-1} := \{\theta \in \mathbb{R}^d \mid \|\theta\|_2^2 = 1\}$ and denote $\mathcal{U}(\mathbb{S}^{d-1})$ as the uniform distribution over it. The set of all probability measures on a given set \mathcal{X} is represented by $\mathcal{P}(\mathcal{X})$. For $p \geq 1$, we denote by $\mathcal{P}_p(\mathcal{X})$ the collection of probability measures on \mathcal{X} that possess finite p -moments. For two sequences a_n and b_n , the notation $a_n = \mathcal{O}(b_n)$ signifies that there exists a universal constant C such that $a_n \leq Cb_n$ for all $n \geq 1$. The pushforward measure of μ under a function $f : \mathbb{R}^d \rightarrow \mathbb{R}$ defined as $f(x) = \theta^\top x$ is denoted by $\theta\#\mu$. For a vector $X \in \mathbb{R}^{dm}$, where $X = (x_1, \dots, x_m)$, the empirical measure associated with X is given by $P_X := \frac{1}{m} \sum_{i=1}^m \delta_{x_i}$.

2 Preliminaries

We first review definitions and computational properties of Wasserstein distance and SW distance.

Wasserstein distance. For the order $p \geq 1$, the Wasserstein- p distance [53, 43] between two distributions $\mu \in \mathcal{P}_p(\mathbb{R}^d)$ and $\nu \in \mathcal{P}_p(\mathbb{R}^d)$ (dimension $d \geq 1$) is defined as:

$$W_p^p(\mu, \nu) = \inf_{\pi \in \Pi(\mu, \nu)} \int_{\mathcal{X} \times \mathcal{Y}} \|x - y\|_p^p d\pi(x, y), \quad (1)$$

where $\Pi(\mu, \nu)$ is the set of all transportation plans i.e., joint distributions which have marginals be two comparing distributions. When μ and ν are discrete distributions i.e., $\mu = \sum_{i=1}^n \alpha_i \delta_{x_i}$ ($n \geq 1$) and $\nu = \sum_{j=1}^m \beta_j \delta_{y_j}$ ($m \geq 1$) where $\sum_{i=1}^n \alpha_i = \sum_{j=1}^m \beta_j = 1$ and $\alpha_i \geq 0, \beta_j \geq 0$ for all $i = 1, \dots, n$ and $j = 1, \dots, m$, Wasserstein distance between μ and ν defined as follows:

$$W_p^p(\mu, \nu) = \min_{\gamma \in \Gamma(\alpha, \beta)} \sum_{i=1}^n \sum_{j=1}^m \|x_i - y_j\|_p^p \gamma_{ij}, \quad (2)$$

where $\Gamma(\alpha, \beta) = \{\gamma \in \mathbb{R}_+^{n \times m} \mid \gamma \mathbf{1} = \alpha, \gamma^\top \mathbf{1} = \beta\}$. Without losing generality, we assume that $n \geq m$. Therefore, the time complexity for solving this linear programming is $\mathcal{O}(n^3 \log n)$ [43], and $\mathcal{O}(n^2)$ in turn which are very expensive. Moreover, from [18], we have the following sample complexity: $\mathbb{E}[|W_p(\mu_n, \nu_m) - W_p(\mu, \nu)|] = \mathcal{O}(\min\{n, m\}^{-1/d})$ here μ_n and ν_m are empirical distributions over n and m i.i.d samples from μ and ν in turn. The above result implies that we need $\min\{n, m\}$ to be large in high-dimension in order to reduce the approximation error. However, as discussed, Wasserstein scales poorly with n and m . Therefore, sliced Wasserstein [45, 9] (SW) is proposed as an alternative solution. The key idea of SW is to utilize the closed-form solution of optimal transport in one-dimension.

One-dimensional Optimal Transport. Given $\mu \in \mathcal{P}(\mathbb{R})$ and $\nu \in \mathcal{P}(\mathbb{R})$, we have the optimal transport mapping from μ to ν is $F_\nu^{-1} \circ F_\mu$ [10, 43] where F_μ and F_ν are CDF of μ and ν respectively. The one-dimensional Wasserstein distance between μ and ν is then defined as follows:

$$\begin{aligned} W_p^p(\mu, \nu) &= \int_{\mathbb{R}} |x - F_\nu^{-1}(F_\mu(x))|^p d\mu(x) \\ &= \int_0^1 |F_\mu^{-1}(q) - F_\nu^{-1}(q)|^p dq, \end{aligned} \quad (3)$$

When μ and ν are discrete distributions i.e., $\mu = \sum_{i=1}^n \alpha_i \delta_{x_i}$ ($n \geq 1$) and $\nu = \sum_{j=1}^m \beta_j \delta_{y_j}$ ($m \geq 1$), quantile functions of μ and ν can be written as follows:

$$\begin{aligned} F_\mu^{-1}(z) &= \sum_{i=1}^n x_{(i)} I \left(\sum_{j=1}^{i-1} \alpha_{(j)} \leq z \leq \sum_{j=1}^i \alpha_{(j)} \right), \\ F_\nu^{-1}(z) &= \sum_{j=1}^m y_{(j)} I \left(\sum_{i=1}^{j-1} \beta_{(i)} \leq z \leq \sum_{i=1}^j \beta_{(i)} \right), \end{aligned}$$

where $x_{(1)} \leq \dots \leq x_{(n)}$ and $y_{(1)} \leq \dots \leq y_{(m)}$ are order statistics. This construction of quantile functions are equivalent to northwest corner algorithm for discrete optimal transport [43, 36]. Therefore, computing one-dimensional Wasserstein distance only cost $\mathcal{O}(n \log n)$ and $\mathcal{O}(n)$ in time complexity and space complexity respectively (assuming $m \leq n$).

Sliced Wasserstein Distance. For $p \geq 1$, the *Sliced Wasserstein (SW)* distance [9] of p -th order between two distributions $\mu \in \mathcal{P}(\mathbb{R}^d)$ and $\nu \in \mathcal{P}(\mathbb{R}^d)$ is defined as:

$$SW_p^p(\mu, \nu) = \mathbb{E}_{\theta \sim \mathcal{U}(\mathbb{S}^{d-1})} [W_p^p(\theta_{\#}\mu, \theta_{\#}\nu)], \quad (4)$$

where $\theta_{\#}\mu$ and $\theta_{\#}\nu$ are the one-dimensional push-forward distributions by applying Radon Transform (RT) [21] on the pdf of μ and ν with the projecting direction θ i.e., $\mathcal{R}_\theta(x) = \theta^\top x$. Using the closed-form of 1DW, we can further rewrite:

$$\begin{aligned} SW_p^p(\mu, \nu) &= \mathbb{E}_{\theta \sim \mathcal{U}(\mathbb{S}^{d-1})} \left[\int_0^1 |F_{\theta_{\#}\mu}^{-1}(q) - F_{\theta_{\#}\nu}^{-1}(q)|^p dq \right], \end{aligned} \quad (5)$$

which boils down to the expectation of difference between two quantile functions of projected distributions. This observation is the key insight in design later streaming estimator of SW (Stream-SW).

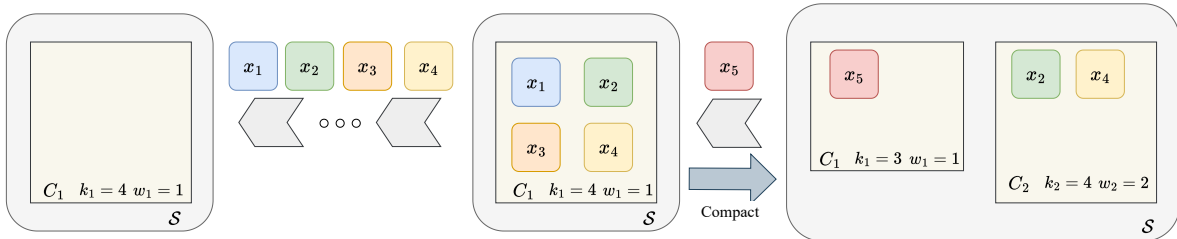


Figure 1: The figure shows the compacting process of a KKL sketch.

Due to the intractability of the expectation in Equation 4, numerical approximation need to be used [37, 27, 48]. For example, Monte Carlo estimation with $\theta_1, \dots, \theta_L \stackrel{i.i.d}{\sim} \mathcal{U}(\mathbb{S}^{d-1})$ ($L \geq 1$) is often used:

$$\widehat{SW}_p^p(\mu, \nu; L) = \frac{1}{L} \sum_{l=1}^L W_p^p(\theta_l \sharp \mu, \theta_l \sharp \nu), \quad (6)$$

where L is often referred to as the number of projections. The time complexity and space complexity of SW are $\mathcal{O}(Ln \log n + Ldn)$ and $\mathcal{O}(Ld + nd)$ in turn. Moreover, from [35, 32, 38, 41, 5], we have that $\mathbb{E}[|SW_p(\mu_n, \nu_m) - SW_p(\mu, \nu)|] = \mathcal{O}(\min\{n, m\}^{-1/2})$. Therefore, SW is statistical scalable and computational scalable in both the number of supports and the number of dimensions.

3 Streaming Sliced Optimal Transport

In this section, we discuss computing sliced optimal transport from sample streams. In greater detail, we receive samples x_1, \dots, x_n ($n > 1$) and y_1, \dots, y_m ($m > 1$) in a streaming fashion in arbitrary order from two interested $d > 1$ dimensional distributions μ and ν , respectively. The goal is to form an approximation of the sliced optimal transport between μ and ν with a *budget-constrained* memory. The constraint comes from the nature of the streaming setting where storing all samples is impractical since n and m are often very large and might be unknown.

3.1 Quantile Sketch

As discussed in Section 2, the key computation of one-dimensional optimal transport and sliced optimal transport (SOT) rely on evaluating CDFs and quantile functions. To enable computing SOT from sample streams, it is a must to compute CDFs and quantile functions from sample streams. The key technique for such task is to build a data structure, named *quantile sketch*, which can yield an approximate number for any quantile query input.

Quantile Sketch. Quantile sketch \mathcal{S} is a data structure that store a subset of samples from the data streams [20, 23]. In this work, we focus on using the KKL sketch [23] which is the optimal randomized comparison-based quantile sketch. In addition, KKL sketch is also mergeable which allows distributed computation. The key component of an KKL sketch is a *compactor* C which is a set of k elements with an associated weight w i.e., $C = \{x_1, \dots, x_k\}$. A compactor, as its name, can compact its k elements into $k/2$ elements of weight $2w$. In greater detail, the items are first sorted. Then, either the even or the odd elements in the set are chosen. For the KKL sketch, there are H hierarchical compactors indexed by their height i.e., C_h for $h = 1, \dots, H$. The associated weight of

C_h is $w_h = 2^{h-1}$. For the capacity of C_h , $k_h = \lceil k(c)^{H-h} \rceil + 1$ ($c = 2/3$) for a given initial capacity k . When the compactor C_h does compaction (triggered when it reaches its capacity), the chosen elements are put into the compactor C_{h+1} . It is worth noting that if k_h is odd, the compaction is conducted only on $k - 1$ first items after sorting to make sure that the total weights is still n . An example of the compacting process of a KKL sketch is shown in Figure 1.

Complexities of KKL sketch. Given a stream of $n > k$ samples, we know that the second compactor from the top compacted its elements at least once, we have $n \geq k_{H-1}w_{H-1} = k_{H-1}2^{H-2}$ which gives $H \leq \log(n/k_{H-1}) + 2 \leq \log((3n)/(2k)) + 2$. The total capacity of all compactors $\sum_{h=1}^H k_h \leq \sum_{h=1}^H (k(2/3)^{H-h} + 2) \leq 3k + 2H \leq 3k + 2(\log((3n)/(2k)) + 2)$ which yields the space complexity of $\mathcal{O}(k + \log(n/k))$. For the time complexity, we know that $H \leq \log(n/(2k/3)) + 2$ and the number of compact operations at the height h i.e., $m_h \leq n/(k_h w_h) \leq (2n)/(k2^h)3^{H-h} \leq 3^{H-h-1}$ ($k_h \geq k/3^{H-h}$ and $w_h = 2^{h-1}$). Therefore, the time complexity for compacting is $\mathcal{O}(\sum_{h=1}^H k_h m_h) = \mathcal{O}(\sum_{h=1}^H (k(2/3)^{H-h} + 2)3^{H-h-1}) = \mathcal{O}(k + n/k)$.

3.2 Streaming CDF and Quantile Function Estimation

Given the quantile sketch, we can form a discrete distribution from samples and their weights from the sketch. The discrete distribution is $\frac{1}{n} \sum_{h=1}^H \sum_{x \in C_h} w_h \delta_x$. With this distribution, we can form streaming estimations of CDF and quantile function.

Streaming CDF estimation. We form the following estimation of CDF from a sketch \mathcal{S} :

$$F_{\mathcal{S}}(y) = \frac{1}{n} \sum_{h=1}^H \sum_{x \in C_h} w_h I(x \leq y). \quad (7)$$

In [23], authors discuss the guarantee for ranking approximation of the quantile sketch. We extend that discussion to the approximation guarantee of the CDF:

Proposition 1. *Given $\mathcal{S}_{\mu,k}$ be the quantile sketch with initial size $k > 0$ constructed from streaming samples x_1, \dots, x_n from $\mu \in \mathcal{P}(\mathbb{R})$, the following probability bound holds:*

$$\mathbb{P}\left(|F_{\mathcal{S}_{\mu,k}}(x) - F_n(x)| > \epsilon\right) \leq 2 \exp(-Ck^2\epsilon^2), \quad (8)$$

$\forall x \in \mathbb{R}$, where $C > 0$ is a constant. When μ has compact support with diameter $R > 0$, the following probability bound holds:

$$\begin{aligned} & \mathbb{P}\left(\int_{\mathbb{R}} |F_{\mathcal{S}_{\mu,k}}(x) - F_n(x)| dx > \epsilon\right) \\ & \leq 2 \exp(-C_R k^2 \epsilon^2), \end{aligned} \quad (9)$$

where $C_R > 0$ is a constant which depends on R .

The proof of Proposition 1 is given in Appendix A.1. From Proposition 1, let $C_R \exp(-k^2\epsilon^2) = \delta$, we need $k = \mathcal{O}((1/\epsilon)\sqrt{\log(2/\delta)})$ to have ϵ error with failure probability δ .

Streaming quantile function estimation. Similar to the case of CDF, we can also form an estimation of the quantile function:

$$F_{\mathcal{S}_{\mu,k}}^{-1}(q) = \inf\{x : F_{\mathcal{S}_{\mu,k}}(x) \geq q\}. \quad (10)$$

We again can guarantee the quality of the approximation of the quantile function as follows:

Proposition 2. *Given \mathcal{S} be the quantile sketch with initial size $k > 1$ constructed from streaming samples x_1, \dots, x_n from $\mu \in \mathcal{P}(\mathbb{R})$, the following probability bound holds:*

$$\begin{aligned} \mathbb{P}\left(\left|F_{\mathcal{S}_{\mu,k}}^{-1}(q) - F_n^{-1}(q)\right| > \epsilon\right) \\ \leq 2 \exp\left(-Ck^2\gamma_{q,\epsilon}^2\right), \end{aligned} \quad (11)$$

$\forall q \in [0, 1]$, where $C > 0$ is a constant and $\gamma_{q,\epsilon} = \min\{q - F_n(F_n^{-1}(q) - \epsilon), F_n(F_n^{-1}(q) + \epsilon) - q\}$. When μ has compact support with diameter $R > 0$, the following probability bound holds:

$$\begin{aligned} \mathbb{P}\left(\int_{\mathbb{R}} |F_{\mathcal{S}_{\mu,k}}^{-1}(x) - F_n^{-1}(x)| dx > \epsilon\right) \\ \leq 2 \exp\left(-C_R k^2 \epsilon^2\right), \end{aligned} \quad (12)$$

where $C_R > 0$ is a constant which depends on R .

The proof of Proposition 2 is given in Appendix A.2. From Proposition 2, we also need $k = \mathcal{O}((1/\epsilon)\sqrt{\log(2/\delta)})$ to have ϵ error with failure probability δ .

Streaming one-dimensional Wasserstein distance. With the discussed streaming estimator for quantile functions, we are able to define a streaming estimator for IDW. We are given x_1, \dots, x_n ($n > 1$) and y_1, \dots, y_m ($m > 1$) in a streaming fashion and in arbitrary order from two interested one-dimensional distributions μ and ν . Let μ_n and ν_m be the two corresponding empirical distributions i.e., $\mu_n = \frac{1}{n} \sum_{i=1}^n \delta_{x_i}$ and $\nu_m = \frac{1}{m} \sum_{j=1}^m \delta_{y_j}$, from the sample streams, we build KKL sketches \mathcal{S}_{μ_n, k_1} and \mathcal{S}_{ν_m, k_2} . After that, we can form the approximation of the one-dimensional Wasserstein distance between μ_n and ν_m as follows:.

Definition 1. *Given two empirical distributions μ_n and ν_m observed in a streaming fashion, and their corresponding quantile sketches \mathcal{S}_{μ_n, k_1} and \mathcal{S}_{ν_m, k_2} with $k_1 > 1$ and $k_2 > 1$, streaming one-dimensional Wasserstein is defined as follow:*

$$\begin{aligned} \widetilde{W}_p^p(\mu_n, \nu_m; \mathcal{S}_{\mu_n, k_1}, \mathcal{S}_{\nu_m, k_2}) \\ = \int_0^1 \left|F_{\mathcal{S}_{\mu_n, k_1}}^{-1}(q) - F_{\mathcal{S}_{\nu_m, k_2}}^{-1}(q)\right|^p dq. \end{aligned} \quad (13)$$

We can rewrite streaming one-dimensional Wasserstein as: $\widetilde{W}_p^p(\mu_n, \nu_m; \mathcal{S}_{\mu_n, k_1}, \mathcal{S}_{\nu_m, k_2}) = W_p^p(\mu_{\mathcal{S}_{\mu_n, k_1}}, \nu_{\mathcal{S}_{\nu_m, k_2}})$, where $\mu_{\mathcal{S}} = \frac{1}{n} \sum_{h=1}^H \sum_{x \in C_h} w_h \delta_x$ denotes the discrete distribution over the quantile sketch \mathcal{S} . In addition, we can also define one-sided streaming one-dimensional Wasserstein by using only a quantile sketch for one distribution. Next, we discuss approximation guarantee of the proposed streaming estimator.

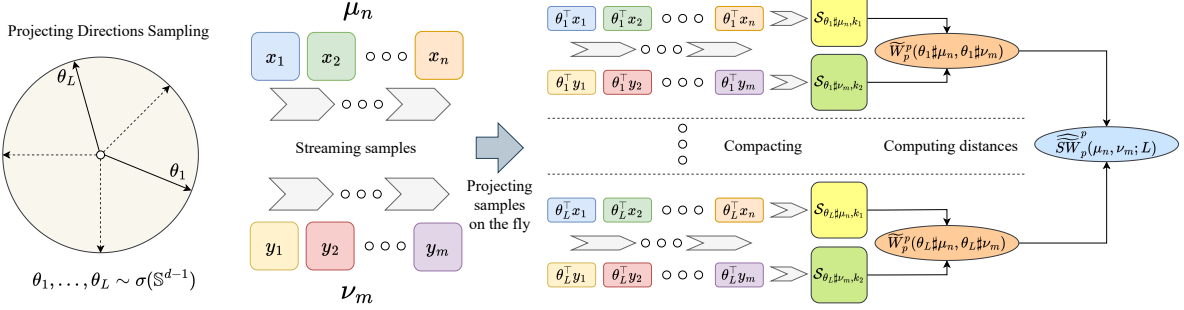


Figure 2: The figure shows the computational procedure of Stream-SW. In the figure, we denotes $\widetilde{W}_p^p(\mu_n, \nu_m; \mathcal{S}_{\mu_n, k_1}, \mathcal{S}_{\nu_m, k_2})$ as $\widetilde{W}_p^p(\mu_n, \nu_m)$ and $\widehat{\widetilde{W}}_p^p(\mu_n, \nu_m; k_1, k_2, L)$ as $\widehat{SW}_p^p(\mu_n, \nu_m; L)$.

Proposition 3. Let $\mu, \nu \in \mathcal{P}(\mathbb{R})$ be probability measures supported on an interval of diameter $R > 0$. Let μ_n and ν_m denote the empirical measures formed from n and m i.i.d. samples from μ and ν , respectively. Let \mathcal{S}_{μ_n, k_1} and \mathcal{S}_{ν_m, k_2} be quantile sketches of initial sizes $k_1, k_2 > 0$ constructed from the samples defining μ_n and ν_m . For any $p \geq 1$ and $\epsilon > 0$, the following bounds hold:

$$\begin{aligned} & \mathbb{P}\left(\left|\widetilde{W}_p^p(\mu_n, \nu_m; \mathcal{S}_{\mu_n, k_1}, \mathcal{S}_{\nu_m, k_2}) - W_p^p(\mu_n, \nu_m)\right| > \epsilon\right) \\ & \leq 4 \exp(-C_{p,R} \min\{k_1^2, k_2^2\} \epsilon^2), \end{aligned} \quad (14)$$

where $C_{p,R} > 0$ is a constant depending only on p and R ,

$$\begin{aligned} & \mathbb{P}\left(\left|\widetilde{W}_p^p(\mu_n, \nu_m; \mathcal{S}_{\mu_n, k_1}, \mathcal{S}_{\nu_m, k_2}) - W_p^p(\mu, \nu)\right| > \epsilon\right) \\ & \leq 8 \exp(-c_{p,R} \min\{k_1^2, k_2^2, n, m\} \epsilon^2), \end{aligned} \quad (15)$$

where $c_{p,R} > 0$ is a constant depending only on p and R .

The proof of Proposition 3 is given in Appendix A.3. When $\min\{k_1, k_2, \sqrt{n}, \sqrt{m}\} = \mathcal{O}((1/\epsilon)\sqrt{\log(8/\delta)})$, we have ϵ error with failure probability δ .

Streaming one-dimensional transport map. Let \mathcal{S}_{μ_n, k_1} and \mathcal{S}_{ν_m, k_2} be quantile sketches of sizes k_1, k_2 constructed from i.i.d. samples drawn from μ and ν , respectively. Define the monotone transport map

$$T_{\mu \rightarrow \nu}(x) := F_\nu^{-1}(F_\mu(x)),$$

and its sketched approximation

$$\widetilde{T}(x) := F_{\mathcal{S}_{\nu_m, k_2}}^{-1}\left(F_{\mathcal{S}_{\mu_n, k_1}}(x)\right).$$

We can also guarantee the approximation of $\widetilde{T}(x)$ under an assumption about the continuity of ν :

Proposition 4. Let $\mu, \nu \in \mathcal{P}(\mathbb{R})$ be probability measures supported on an interval of diameter $R > 0$. Assume that ν is absolutely continuous with density f_ν satisfying $f_\nu(x) \geq m > 0$ for a.e. $x \in \mathbb{R}$. Then for any $\epsilon > 0$,

$$\begin{aligned} & \mathbb{P}\left(\int_{\mathbb{R}} |\widetilde{T}(x) - T_{\mu \rightarrow \nu}(x)| d\mu(x) > \epsilon\right) \\ & \leq 8 \exp(-c_{m,R} \epsilon^2 \min\{k_1, k_2\}), \end{aligned} \quad (16)$$

where $c_{m,R} > 0$ depends only on m and R .

3.3 Streaming Sliced Wasserstein

With the previously discussed streaming estimator of quantile function, we can define Stream-SW as follows:

Definition 2. Let $k_1 > 1$, $k_2 > 1$, and $p \geq 1$. The streaming Sliced Wasserstein (*Stream-SW*) distance between two empirical distributions $\mu_n \in \mathcal{P}_p(\mathbb{R}^d)$ and $\nu_m \in \mathcal{P}_p(\mathbb{R}^d)$, whose supports are observed in a streaming manner, is defined by

$$\begin{aligned} & \widetilde{SW}_p^p(\mu_n, \nu_m; k_1, k_2) \\ &= \mathbb{E}_{\theta \sim \sigma} \left[\widetilde{W}_p^p(\theta_{\#} \mu_n, \theta_{\#} \nu_m; S_{\theta_{\#} \mu_n, k_1}, S_{\theta_{\#} \nu_m, k_2}) \right], \end{aligned} \quad (17)$$

where $\sigma \in \mathcal{P}(\mathbb{S}^{d-1})$ is a slicing distribution on the unit sphere and $\widetilde{W}_p^p(\theta_{\#} \mu_n, \theta_{\#} \nu_m; S_{\theta_{\#} \mu_n, k_1}, S_{\theta_{\#} \nu_m, k_2})$ is defined in Definition 1.

From the failure probability of streaming quantile estimator in Proposition 3, we obtain similar result for Stream-SW.

Corollary 1. Let $\mu, \nu \in \mathcal{P}_p(\mathbb{R}^d)$ be probability measures supported on a compact set of diameter $R > 0$. Let μ_n and ν_m be the empirical measures formed from n and m i.i.d. samples from μ and ν , respectively. Let $k_1 > 1$, $k_2 > 1$, and let $S_{\theta_{\#} \mu_n, k_1}$ and $S_{\theta_{\#} \nu_m, k_2}$ be quantile sketches constructed from streaming observations of the projected empirical measures $\theta_{\#} \mu_n$ and $\theta_{\#} \nu_m$ where $\theta \in \mathbb{S}^{d-1}$. Then for any $p \geq 1$ and $\epsilon > 0$, the following probability bounds hold:

$$\begin{aligned} & \mathbb{P} \left(\left| \widetilde{SW}_p^p(\mu_n, \nu_m; k_1, k_2) - SW_p^p(\mu_n, \nu_m) \right| > \epsilon \right) \\ & \leq 4 \exp(-C_{p,R} \min\{k_1^2, k_2^2\} \epsilon^2), \end{aligned} \quad (18)$$

where $C_{p,R} > 0$ is a constant depending only on p and R ,

$$\begin{aligned} & \mathbb{P} \left(\left| \widetilde{SW}_p^p(\mu_n, \nu_m; k_1, k_2) - SW_p^p(\mu, \nu) \right| > \epsilon \right) \\ & \leq 8 \exp(-c_{p,R} \min\{k_1^2, k_2^2, n, m\} \epsilon^2), \end{aligned} \quad (19)$$

where $c_{p,R} > 0$ is a constant depending only on p and R .

The proof of Corollary 1 is given in Appendix A.6.

Numerical approximation. As in the conventional SW, we need to approximate the expectation in Definition 2. There are some existing options such as Monte Carlo (MC) estimation [9] and quasi-Monte Carlo approximation and randomized quasi-Monte Carlo estimation [37]. We refer the reader to a recent guide in [48] for a detailed discussion. By using one of the mentioned constructions, we can obtain a final set of projecting directions $\theta_1, \dots, \theta_L \in \mathbb{S}^{d-1}$ with $L > 0$ which is referred to as the number of projections. We then can form the numerical approximation of streaming SW as follows:

$$\begin{aligned} & \widehat{SW}_p^p(\mu_n, \nu_m; k_1, k_2, L) \\ &= \frac{1}{L} \sum_{l=1}^L \widetilde{W}_p^p(\theta_l \# \mu_n, \theta_l \# \nu_m; S_{\theta_l \# \mu_n, k_1}, S_{\theta_l \# \nu_m, k_2}). \end{aligned} \quad (20)$$

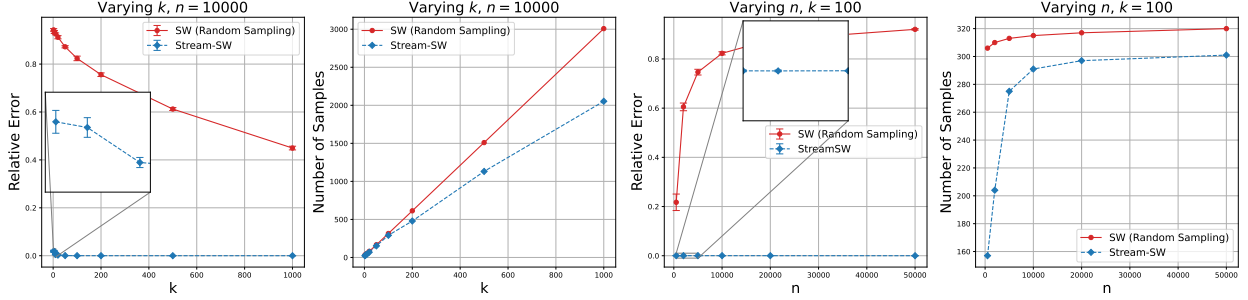


Figure 3: Relative errors and number of samples when comparing mixtures of Gaussian distributions.

We present the computational process of Stream-SW in Figure 2. For simplicity, we use MC estimation in this work i.e., $\theta_1, \dots, \theta_L \stackrel{i.i.d.}{\sim} \sigma(\mathbb{S}^{d-1})$. We then discuss the final theoretical guarantee result for the MC estimation.

Theorem 1. *Let $\mu, \nu \in \mathcal{P}_p(\mathbb{R}^d)$ be probability measures supported on a compact set of diameter $R > 0$. Let μ_n and ν_m be the empirical measures formed from n and m i.i.d. samples from μ and ν , respectively. Let $k_1 > 1$, $k_2 > 1$, and let $S_{\theta_{\sharp}\mu_n, k_1}$ and $S_{\theta_{\sharp}\nu_m, k_2}$ be quantile sketches constructed from streaming observations of the projected empirical measures $\theta_{\sharp}\mu_n$ and $\theta_{\sharp}\nu_m$, where $\theta \in \mathbb{S}^{d-1}$. Then for any $p \geq 1$ and $\epsilon > 0$, the following probability bound holds:*

$$\begin{aligned} & \mathbb{P}\left(\left|\widehat{SW}_p^p(\mu_n, \nu_m; k_1, k_2, L) - SW_p^p(\mu, \nu)\right| > \epsilon\right) \\ & \leq 10 \exp(-c'_{p,R} \min\{k_1^2, k_2^2, n, m, L\} \epsilon^2), \end{aligned} \quad (21)$$

where $c'_{p,R} > 0$ is a constant depending only on p and R .

The proof of Theorem 1 is given in Appendix A.5. When $\min\{k_1, k_2, \sqrt{n}, \sqrt{m}, \sqrt{L}\} = \mathcal{O}((1/\epsilon)\sqrt{\log(10/\delta)})$, we have ϵ error with failure probability δ .

Computational complexities. Without losing generality, we assume that $k_1 \leq k_2 \leq k$, from the discussion of the space complexity of KKL sketches in Section 3.1, the space complexity of Stream-SW is $\mathcal{O}(L(k + \log(n/k)) + Ld)$ where Ld is for storing projecting directions $\theta_1, \dots, \theta_L$. The time complexity for compacting is $\mathcal{O}(L \sum_{h=1}^H k_h m_h) = \mathcal{O}(L \sum_{h=1}^H (k(2/3)^{H-h} + 2)3^{H-h-1}) = \mathcal{O}(Lk + Ln/k)$. For computing 1DW, the time complexity is $\mathcal{O}(L(k + \log(n/k)) \log((k + \log(n/k))))$. Adding time complexity for projection $\mathcal{O}(Ldn)$, we have the final time complexity $\mathcal{O}(L(k + \log(n/k)) \log(k + \log(n/k)) + Lk + Ln/k + Ldn)$. In summary, the time complexity of Stream-SW is linear in n and is near linear in k and the space complexity of Stream-SW is logarithmic in n and is linear in k .

4 Experiments

4.1 Approximation Error Analysis

We first analyze the approximation error of Stream-SW. We simulate samples from the following two mixtures of Gaussians $\mu_1 = 0.3\mathcal{N}\left(\begin{bmatrix} 0.0 \\ 0.0 \end{bmatrix}, \begin{bmatrix} 0.5 & 0.2 \\ 0.2 & 0.5 \end{bmatrix}\right) + 0.4\mathcal{N}\left(\begin{bmatrix} 3.0 \\ 3.0 \end{bmatrix}, \begin{bmatrix} 0.8 & -0.3 \\ -0.3 & 0.5 \end{bmatrix}\right) +$

Table 1: Summary of Wasserstein-2 scores [16] (multiplied by 10^3) from three different runs.

Loss	Step 0	Step 500	Step 1000	Step 2000	Step 3000	Step 4000	Step 5000
SW L=100 (Full)	204.83 ± 0.0	89.12 ± 0.0	26.78 ± 0.0	1.9 ± 0.0	0.94 ± 0.0	0.87 ± 0.0	0.84 ± 0.0
SW L=1000 (Full)	204.83 ± 0.0	88.98 ± 0.0	26.62 ± 0.0	1.63 ± 0.0	0.31 ± 0.0	0.08 ± 0.0	0.01 ± 0.0
SW L=100 k=100 (Sampling)	204.83 ± 0.0	90.83 ± 1.3	31.1 ± 1.05	9.8 ± 1.33	9.37 ± 1.42	9.37 ± 1.45	9.36 ± 1.46
Stream-SW L=100 k=100	204.83 ± 0.0	89.14 ± 0.04	26.94 ± 0.07	3.01 ± 0.03	2.1 ± 0.02	1.97 ± 0.03	1.93 ± 0.03
SW L=100 k=200 (Sampling)	204.83 ± 0.0	90.32 ± 0.92	29.54 ± 0.62	7.19 ± 2.53	6.68 ± 2.84	6.64 ± 2.89	6.63 ± 2.9
Stream-SW L=100 k=200	204.83 ± 0.0	89.14 ± 0.01	26.84 ± 0.01	2.31 ± 0.01	1.46 ± 0.01	1.38 ± 0.01	1.36 ± 0.02
SW L=1000 k=100 (Sampling)	204.83 ± 0.0	90.69 ± 1.28	30.9 ± 1.08	9.58 ± 1.41	9.42 ± 1.57	9.53 ± 1.58	9.59 ± 1.58
Stream-SW L=1000 k=100	204.83 ± 0.0	89.08 ± 0.01	26.85 ± 0.01	2.5 ± 0.01	1.17 ± 0.01	0.93 ± 0.03	0.85 ± 0.03
SW L=1000 k=200 (Sampling)	204.83 ± 0.0	90.17 ± 0.92	29.37 ± 0.63	6.99 ± 2.61	6.57 ± 2.98	6.59 ± 3.05	6.59 ± 3.06
Stream-SW L=1000 k=200	204.83 ± 0.0	89.0 ± 0.0	26.67 ± 0.01	1.93 ± 0.01	0.73 ± 0.01	0.54 ± 0.01	0.48 ± 0.01

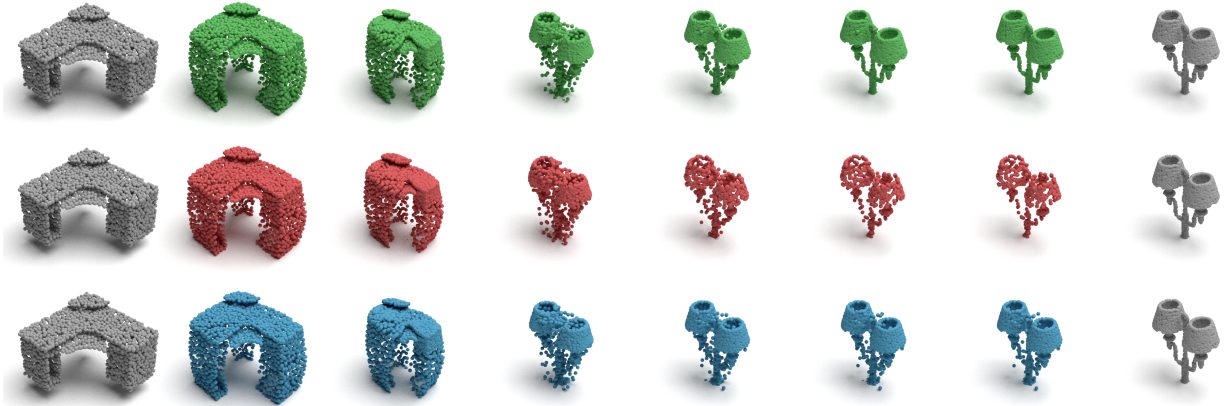


Figure 4: Gradient flows from Full SW, SW with random sampling, and Stream-SW in turn.

$0.3\mathcal{N}\left(\begin{bmatrix} -3.0 \\ 3.0 \end{bmatrix}, \begin{bmatrix} 0.6 & 0.1 \\ 0.1 & 0.6 \end{bmatrix}\right)$, and $\mu_2 = 0.4\mathcal{N}\left(\begin{bmatrix} -3.0 \\ -3.0 \end{bmatrix}, \begin{bmatrix} 0.7 & 0.1 \\ 0.1 & 0.7 \end{bmatrix}\right) + 0.3\mathcal{N}\left(\begin{bmatrix} 3.0 \\ -3.0 \end{bmatrix}, \begin{bmatrix} 0.5 & -0.2 \\ -0.2 & 0.5 \end{bmatrix}\right) + 0.3\mathcal{N}\left(\begin{bmatrix} 0.0 \\ 3.0 \end{bmatrix}, \begin{bmatrix} 0.6 & 0.2 \\ 0.2 & 0.6 \end{bmatrix}\right)$. We investigate the approximation error and the number of samples keeping from the stream when increasing k (sketch size) and n (number of supports). We set the number of projections $L = 1000$, we vary $k \in \{2, 5, 10, 20, 50, 100, 200, 500, 1000\}$ when keeping $n = 1000$, and vary $n \in \{500, 2000, 5000, 10000, 20000, 50000\}$ when keep $k = 100$. We show the relative approximation error (absolute difference of the estimated distance from the true distance divided by the true distance) with 10 different runs in Figure 3. Here, we compare Stream-SW with SW using random sampling to retain $3k + 2\log(n/(2k/3))$ samples (the upper bound of the KKL sketch’s number of samples). We see that Stream-SW can achieve significantly better relative error and requires fewer samples. We observe the same phenomenon with Gaussian distributions in C.

4.2 Streaming Point-cloud Classification

We follow the setup in [28]. In particular, we select (stratified sampling from 10 categories) 500 point clouds as the training set and 300 point clouds as the testing set from the ModelNet10 dataset [56]. For point cloud, we sample 500 points. After that, we use the K-NN algorithm with $K = 5$ neighbors to evaluate the classification accuracy on the testing set. We vary the sketch size $k \in \{5, 10, 20, 50\}$ and the number of projections $L \in \{5, 10, 50, 100\}$. We show the result for Stream-SW, SW with the

Table 2: Point-cloud classification test accuracy via K-nearest neighbors.

L	SW (Full)	SW (Random Sampling)				Stream-SW			
		$k = 5$	$k = 10$	$k = 20$	$k = 50$	$k = 5$	$k = 10$	$k = 20$	$k = 50$
$L = 5$	68.33	39.33	51.67	56	61.33	45.53	45.33	63.33	68.67
$L = 10$	73.33	47.67	55.33	62	68	52.67	69.33	73	73
$L = 50$	77.33	54	63.67	67.67	73.33	70	73.67	76.33	77.67
$L = 100$	77.67	56.67	62	68	72.67	72.33	76.67	77.67	77.67

Table 3: Delay (Early) time for detecting the transition in MSRC-12 that corresponds to four users.

Guest 1		Guest 2		Guest 3		Guest 4	
SW	Stream-SW	SW	Stream-SW	SW	Stream-SW	SW	Stream-SW
100	50	100	10	49	24	100	32

random sampling of $3k + 2 \log(n/(2k/3))$ samples, and Full SW (keeping all samples) in Table 2. From the table, we see that Stream-SW can lead to considerably higher classification accuracy than SW for any choices of L and k , especially when having small k e.g., 5, 10. Stream-SW can lead to comparable accuracies when having large enough k e.g., 20. When the number of projections is large enough e.g., $L = 100$, Stream-SW can lead to comparable accuracy to Full SW with $k = 10$.

4.3 Streaming Gradient Flow

We model a distribution $\mu(t)$ flowing with time t along the gradient flow of a loss functional $\mu(t) \rightarrow SW_2(\mu(t), \nu)$ that drives it towards a target distribution ν [46]. We consider discrete flows, namely, $\mu(t) = \frac{1}{n} \sum_{i=1}^n \delta_{x_i(t)}$ and $\nu = \frac{1}{n} \sum_{i=1}^n \delta_{y_i}$. Here, ν is assumed to be received from a sample stream. We refer to Appendix B for the detail about one-sided streaming sliced Wasserstein which is the case here. We choose $\mu(0)$ and ν as two point-cloud shapes in the ShapeNet Core-55 dataset [11]. After that, we solve the flows by using the Euler scheme with 5000 iterations, step size 0.001, and approximated gradient as discussed in Appendix B. We show the Wasserstein-2 scores [16] in 3 different runs for Stream-SW, SW with random sampling of $3k + 2 \log(n/(2k/3))$ samples, and Full SW with $L \in \{100, 1000\}$ and $k \in \{100, 200\}$ in Table 1. We see that Stream-SW makes flows converge faster than SW with random sampling. We strengthen the claim by qualitative comparison in Figure 4 with $L = 1000$ and $k = 200$. We visualize flows in other settings in Appendix C.

4.4 Streaming Change Point Detection

We follow the same setup in [55] with a real-world dataset called the Microsoft Research Cambridge-12 (MSRC-12) Kinect gesture dataset [17]. After pre-processing, this dataset consists of actions from four people, each with 855 samples in \mathbb{R}^{60} , and with a change of action from bending to throwing at the time index 500. The conventional streaming change point detection is based on sliding window with the window size $W = 100$. The null statistic (distance between two consecutive random windows) is computed for 1000 times from data before time index 300 to obtain the true threshold such that the false alarm rate is controlled within $\alpha = 0.05$. In contrast, for Stream-SW, the null statistic is SW between two random subsets with the sizes are set to 100. We trigger a change if the value of Stream-SW is greater than the null statistic. We report the delay/early time in Table 3.

Since Stream-SW is native in streaming settings, it performs much better than SW with sliding window. We refer the reader to Appendix B for more details on detection statistics.

5 Conclusion

We have presented streaming sliced Wasserstein (Stream-SW) which is the first streaming estimator for sliced Wasserstein distance from sample streams. The key idea of Stream-SW is to utilize streaming quantile function approximation based on quantile sketches. We have discussed approximation guarantees and computational complexities of Stream-SW. On the experimental side, we investigate the approximation error of Stream-SW, and compare it with SW using random sampling in streaming point-cloud classification, streaming gradient flow, and streaming change point detection. Future works will extend Stream-SW to other variants of SW such as generalized sliced Wasserstein [24], spherical sliced Wasserstein [6, 52], and sliced Wasserstein on manifolds [8, 39].

References

- [1] P. Achlioptas, O. Diamanti, I. Mitliagkas, and L. Guibas. Learning representations and generative models for 3d point clouds. In *International conference on machine learning*, pages 40–49. PMLR, 2018. (Cited on page 1.)
- [2] L. Ambrogioni, U. Güçlü, Y. Güçlütürk, M. Hinne, M. A. van Gerven, and E. Maris. Wasserstein variational inference. *Advances in Neural Information Processing Systems*, 31, 2018. (Cited on page 1.)
- [3] M. Arjovsky, S. Chintala, and L. Bottou. Wasserstein generative adversarial networks. In *International Conference on Machine Learning*, pages 214–223, 2017. (Cited on page 1.)
- [4] E. Bernton, P. E. Jacob, M. Gerber, and C. P. Robert. Approximate Bayesian computation with the Wasserstein distance. *Journal of the Royal Statistical Society*, 2019. (Cited on page 1.)
- [5] M. T. Boedihardjo. Sharp bounds for max-sliced Wasserstein distances. *Foundations of Computational Mathematics*, pages 1–32, 2025. (Cited on page 5.)
- [6] C. Bonet, P. Berg, N. Courty, F. Septier, L. Drumetz, and M.-T. Pham. Spherical sliced-Wasserstein. *International Conference on Learning Representations*, 2023. (Cited on page 13.)
- [7] C. Bonet, N. Courty, F. Septier, and L. Drumetz. Efficient gradient flows in sliced-Wasserstein space. *Transactions on Machine Learning Research*, 2022. (Cited on page 2.)
- [8] C. Bonet, L. Drumetz, and N. Courty. Sliced-Wasserstein distances and flows on Cartan-Hadamard manifolds. *Journal of Machine Learning Research*, 26(32):1–76, 2025. (Cited on page 13.)
- [9] N. Bonneel, J. Rabin, G. Peyré, and H. Pfister. Sliced and Radon Wasserstein barycenters of measures. *Journal of Mathematical Imaging and Vision*, 1(51):22–45, 2015. (Cited on pages 1, 4, and 9.)

- [10] N. Bonnotte. *Unidimensional and evolution methods for optimal transportation*. PhD thesis, Paris 11, 2013. (Cited on page 4.)
- [11] A. X. Chang, T. Funkhouser, L. Guibas, P. Hanrahan, Q. Huang, Z. Li, S. Savarese, M. Savva, S. Song, H. Su, et al. Shapenet: An information-rich 3d model repository. *arXiv preprint arXiv:1512.03012*, 2015. (Cited on page 12.)
- [12] H. Chen and H.-G. Müller. Sliced Wasserstein regression. *arXiv preprint arXiv:2306.10601*, 2023. (Cited on page 2.)
- [13] M. Cuturi. Sinkhorn distances: Lightspeed computation of optimal transport. In *Advances in Neural Information Processing Systems*, pages 2292–2300, 2013. (Cited on page 1.)
- [14] I. Deshpande, Y.-T. Hu, R. Sun, A. Pyrros, N. Siddiqui, S. Koyejo, Z. Zhao, D. Forsyth, and A. G. Schwing. Max-sliced Wasserstein distance and its use for GANs. In *Proceedings of the IEEE Conference on Computer Vision and Pattern Recognition*, pages 10648–10656, 2019. (Cited on page 28.)
- [15] I. Deshpande, Z. Zhang, and A. G. Schwing. Generative modeling using the sliced Wasserstein distance. In *Proceedings of the IEEE Conference on Computer Vision and Pattern Recognition*, pages 3483–3491, 2018. (Cited on page 2.)
- [16] R. Flamary, N. Courty, A. Gramfort, M. Z. Alaya, A. Boisbunon, S. Chambon, L. Chapel, A. Corenflos, K. Fatras, N. Fournier, L. Gautheron, N. T. Gayraud, H. Janati, A. Rakotomamonjy, I. Redko, A. Rolet, A. Schutz, V. Seguy, D. J. Sutherland, R. Tavenard, A. Tong, and T. Vayer. Pot: Python optimal transport. *Journal of Machine Learning Research*, 22(78):1–8, 2021. (Cited on pages 11 and 12.)
- [17] S. Fothergill, H. Mentis, P. Kohli, and S. Nowozin. Instructing people for training gestural interactive systems. In *Proceedings of the SIGCHI conference on human factors in computing systems*, pages 1737–1746, 2012. (Cited on page 12.)
- [18] N. Fournier and A. Guillin. On the rate of convergence in Wasserstein distance of the empirical measure. *Probability theory and related fields*, 162(3):707–738, 2015. (Cited on pages 1 and 4.)
- [19] Z. Goldfeld, K. Kato, G. Rioux, and R. Sadhu. Statistical inference with regularized optimal transport. *Information and Inference: A Journal of the IMA*, 13(1):iaad056, 2024. (Cited on page 21.)
- [20] M. Greenwald and S. Khanna. Space-efficient online computation of quantile summaries. *ACM SIGMOD Record*, 30(2):58–66, 2001. (Cited on page 5.)
- [21] S. Helgason. The Radon transform on \mathbb{R}^n . In *Integral Geometry and Radon Transforms*, pages 1–62. Springer, 2011. (Cited on pages 1 and 4.)
- [22] X. Hu and Z. Lin. Two-sample distribution tests in high dimensions via max-sliced wasserstein distance and bootstrapping. *Biometrika*, page asaf001, 2025. (Cited on page 2.)
- [23] Z. Karnin, K. Lang, and E. Liberty. Optimal quantile approximation in streams. In *IEEE Symposium on Foundations of Computer Science (FOCS)*, pages 71–78. IEEE, 2016. (Cited on pages 5 and 6.)

- [24] S. Kolouri, K. Nadjahi, U. Simsekli, R. Badeau, and G. Rohde. Generalized sliced Wasserstein distances. In *Advances in Neural Information Processing Systems*, pages 261–272, 2019. (Cited on pages 13 and 28.)
- [25] S. Kolouri, G. K. Rohde, and H. Hoffmann. Sliced Wasserstein distance for learning Gaussian mixture models. In *Proceedings of the IEEE Conference on Computer Vision and Pattern Recognition*, pages 3427–3436, 2018. (Cited on page 2.)
- [26] C.-Y. Lee, T. Batra, M. H. Baig, and D. Ulbricht. Sliced Wasserstein discrepancy for unsupervised domain adaptation. In *Proceedings of the IEEE/CVF Conference on Computer Vision and Pattern Recognition*, pages 10285–10295, 2019. (Cited on page 2.)
- [27] R. Leluc, A. Dieuleveut, F. Portier, J. Segers, and A. Zhuman. Sliced-Wasserstein estimation with spherical harmonics as control variates. In *Proceedings of the 41st International Conference on Machine Learning*, 2024. (Cited on page 5.)
- [28] T. Li, C. Meng, H. Xu, and J. Yu. Hilbert curve projection distance for distribution comparison. *IEEE Transactions on Pattern Analysis and Machine Intelligence*, 46(7):4993–5007, 2024. (Cited on page 11.)
- [29] Y. Lipman, R. T. Chen, H. Ben-Hamu, M. Nickel, and M. Le. Flow matching for generative modeling. In *The Eleventh International Conference on Learning Representations*, 2023. (Cited on page 1.)
- [30] A. Liutkus, U. Simsekli, S. Majewski, A. Durmus, and F.-R. Stöter. Sliced-Wasserstein flows: Nonparametric generative modeling via optimal transport and diffusions. In *International Conference on Machine Learning*, pages 4104–4113. PMLR, 2019. (Cited on page 2.)
- [31] M. Luong, K. Nguyen, N. Ho, R. Haf, D. Phung, and L. Qu. Revisiting deep audio-text retrieval through the lens of transportation. In *The Twelfth International Conference on Learning Representations*, 2024. (Cited on page 1.)
- [32] T. Manole, S. Balakrishnan, and L. Wasserman. Minimax confidence intervals for the sliced Wasserstein distance. *Electronic Journal of Statistics*, 16(1):2252–2345, 2022. (Cited on page 5.)
- [33] A. Mensch and G. Peyré. Online sinkhorn: Optimal transport distances from sample streams. *Advances in Neural Information Processing Systems*, 33:1657–1667, 2020. (Cited on page 2.)
- [34] K. Nadjahi, V. De Bortoli, A. Durmus, R. Badeau, and U. Şimşekli. Approximate Bayesian computation with the sliced-Wasserstein distance. In *ICASSP 2020-2020 IEEE International Conference on Acoustics, Speech and Signal Processing (ICASSP)*, pages 5470–5474. IEEE, 2020. (Cited on page 2.)
- [35] K. Nadjahi, A. Durmus, L. Chizat, S. Kolouri, S. Shahrampour, and U. Simsekli. Statistical and topological properties of sliced probability divergences. *Advances in Neural Information Processing Systems*, 33:20802–20812, 2020. (Cited on page 5.)
- [36] K. Nguyen. An introduction to sliced optimal transport: Foundations, advances, extensions, and applications. *Foundations and Trends® in Computer Graphics and Vision*, 17(3-4):171–406, 2025. (Cited on pages 1 and 4.)

- [37] K. Nguyen, N. Bariletto, and N. Ho. Quasi-monte carlo for 3d sliced Wasserstein. In *The Twelfth International Conference on Learning Representations*, 2024. (Cited on pages 5 and 9.)
- [38] K. Nguyen, N. Ho, T. Pham, and H. Bui. Distributional sliced-Wasserstein and applications to generative modeling. In *International Conference on Learning Representations*, 2021. (Cited on page 5.)
- [39] K. Nguyen and P. Mueller. Summarizing Bayesian nonparametric mixture posterior-sliced optimal transport metrics for Gaussian mixtures. *arXiv preprint arXiv:2411.14674*, 2024. (Cited on pages 2 and 13.)
- [40] K. Nguyen, Y. Ni, and P. Mueller. Bayesian density-density regression with application to cell-cell communications. *arXiv preprint arXiv:2504.12617*, 2025. (Cited on page 2.)
- [41] S. Nietert, R. Sadhu, Z. Goldfeld, and K. Kato. Statistical, robustness, and computational guarantees for sliced Wasserstein distances. *Advances in Neural Information Processing Systems*, 2022. (Cited on page 5.)
- [42] O. Pele and M. Werman. Fast and robust earth mover’s distances. In *2009 IEEE 12th International Conference on Computer Vision*, pages 460–467. IEEE, September 2009. (Cited on page 1.)
- [43] G. Peyré and M. Cuturi. Computational optimal transport: With applications to data science. *Foundations and Trends® in Machine Learning*, 11(5-6):355–607, 2019. (Cited on pages 1, 3, and 4.)
- [44] A.-A. Pooladian, H. Ben-Hamu, C. Domingo-Enrich, B. Amos, Y. Lipman, and R. T. Chen. Multisample flow matching: Straightening flows with minibatch couplings. In *International Conference on Machine Learning*, pages 28100–28127. PMLR, 2023. (Cited on page 1.)
- [45] J. Rabin, S. Ferradans, and N. Papadakis. Adaptive color transfer with relaxed optimal transport. In *2014 IEEE International Conference on Image Processing (ICIP)*, pages 4852–4856. IEEE, 2014. (Cited on page 4.)
- [46] F. Santambrogio. Optimal transport for applied mathematicians. *Birkäuser, NY*, 55(58-63):94, 2015. (Cited on page 12.)
- [47] L. Shi, J. Fan, and J. Yan. Ot-clip: Understanding and generalizing clip via optimal transport. In *Forty-first International Conference on Machine Learning*, 2024. (Cited on page 1.)
- [48] K. Sisouk, J. Delon, and J. Tierny. A user guide to sampling strategies for sliced optimal transport. *arXiv preprint arXiv:2502.02275*, 2025. (Cited on pages 5 and 9.)
- [49] S. Srivastava, C. Li, and D. B. Dunson. Scalable bayes via barycenter in wasserstein space. *Journal of Machine Learning Research*, 19(8):1–35, 2018. (Cited on page 1.)
- [50] I. Tolstikhin, O. Bousquet, S. Gelly, and B. Schoelkopf. Wasserstein auto-encoders. In *International Conference on Learning Representations*, 2018. (Cited on page 1.)

- [51] A. Tong, K. FATRAS, N. Malkin, G. Huguet, Y. Zhang, J. Rector-Brooks, G. Wolf, and Y. Bengio. Improving and generalizing flow-based generative models with minibatch optimal transport. *Transactions on Machine Learning Research*, 2024. Expert Certification. (Cited on page 1.)
- [52] H. Tran, Y. Bai, A. Kothapalli, A. Shahbazi, X. Liu, R. D. Martin, and S. Kolouri. Stereographic spherical sliced Wasserstein distances. *International Conference on Machine Learning*, 2024. (Cited on page 13.)
- [53] C. Villani. *Optimal transport: old and new*, volume 338. Springer Science & Business Media, 2008. (Cited on pages 1 and 3.)
- [54] F. Wang, C. Poon, and T. Shardlow. Compressed online sinkhorn. *arXiv preprint arXiv:2310.05019*, 2023. (Cited on page 2.)
- [55] J. Wang, R. Gao, and Y. Xie. Two-sample test with kernel projected wasserstein distance. In *International Conference on Artificial Intelligence and Statistics*, pages 8022–8055. PMLR, 2022. (Cited on pages 12 and 28.)
- [56] Z. Wu, S. Song, A. Khosla, F. Yu, L. Zhang, X. Tang, and J. Xiao. 3d shapenets: A deep representation for volumetric shapes. In *Proceedings of the IEEE conference on computer vision and pattern recognition*, pages 1912–1920, 2015. (Cited on page 11.)
- [57] M. Yi and S. Liu. Sliced Wasserstein variational inference. In *Fourth Symposium on Advances in Approximate Bayesian Inference*, 2021. (Cited on page 2.)

Supplement to “Streaming Sliced Optimal Transport”

We first provide skipped technical proofs in in Appendix A. We then provide additional materials in Appendix B. Additional experimental results in streaming Gaussian comparison, streaming gradient flows, and streaming change point detection in Appendix C. We report the detail of computational device for experiments in Appendix D.

A Proofs

A.1 Proof of Proposition 1

We denote \mathcal{S} as the quantile sketch with initial size $k > 1$ constructed from streaming samples x_1, \dots, x_n from $\mu \in \mathcal{P}(\mathbb{R})$. We recall that when the top compactor was created, the second compactor from the top compacted its elements at least once. Therefore $n \geq k_{H-1}w_{H-1} = k_{H-1}2^{H-2}$ which gives $H \leq \log(n/k_{H-1}) + 2 \leq \log((3n)/(2k)) + 2$. Using the above we can bound the number of compact operations, $m_h \leq n/(k_h w_h) \leq (2n)/(k2^H)3^{H-h} \leq 3^{H-h-1}$.

Let define $F_n(y) = \frac{1}{n} \sum_{i=1}^n I(x_i \leq y)$, and $F_{\mathcal{S},h}(y) = \frac{1}{n} \sum_{h'=1}^h \sum_{x \in C_{h'}} w_{h'} I(x \leq y)$. We define the error:

$$error(y, h) = F_{\mathcal{S},h}(y) - F_{\mathcal{S},h-1}(y), \quad (22)$$

to be the total change in the the value of CDF of y due to level h . Note that each compaction operation in level h either leaves value of CDF of y unchanged or adds w_h/n or subtracts w_h/n with equal probability. Therefore, $error(x, h) = \sum_{i=1}^{m_h} \frac{w_h}{n} \xi_{i,h}$ where $\xi_{i,h}$ is a Bernoulli random variable with $\mathbb{E}[\xi_{i,h}] = 0$ and $|\xi_{i,h}| \leq 1$. Therefore, the total loss is:

$$F_{\mathcal{S},H}(x) - F_n(x) = \sum_{h=1}^H error(x, h) = \sum_{h=1}^H \sum_{i=1}^{m_h} \frac{w_h}{n} \xi_{i,h} \quad (23)$$

From the Hoeffding’s inequality, we have:

$$\mathbb{P}\left(\sup_{x \in \mathbb{R}} |F_n(x) - F_{\mathcal{S}}(x)| > \epsilon\right) \leq 2 \exp\left(-\frac{n^2 \epsilon^2}{2 \sum_{h=1}^H \sum_{i=1}^{m_h} w_h^2}\right) \quad (24)$$

We further have

$$\begin{aligned} \sum_{h=1}^H \sum_{i=1}^{m_h} w_h^2 &= \sum_{i=1}^H m_h w_h^2 \leq \sum_{h=1}^H (1/3)^{H-h-1} 2^{2h-1} \\ &= \frac{(1/3)^{H-1}}{4} \sum_{h=1}^H (4/3)^h \leq \frac{(1/3)^{H-1}}{4} \frac{(4/3)^H}{(4/3) - 1} \leq \frac{(2/3)}{8(4/3 - 1)} 2^{2H} = 2^{2H-2}. \end{aligned} \quad (25)$$

Since $H \leq \log((3n)/(2k)) + 2$, we obtain

$$\sum_{h=1}^H \sum_{i=1}^{m_h} w_h^2 \leq 2^{2 \log((3n)/(2k)) + 2} = \frac{9n^2}{k^2}. \quad (26)$$

Overall, we have:

$$\mathbb{P}\left(\sup_{x \in \mathbb{R}} |F_n(x) - F_S(x)| > \epsilon\right) \leq 2 \exp(-Ck^2\epsilon^2). \quad (27)$$

Compact support. When having compact support (at most R), we have:

$$\mathbb{P}\left(\int_{\mathbb{R}} |F_n(x) - F_S(x)| dx > \epsilon\right) \leq \mathbb{P}\left(\sup_{x \in \mathbb{R}} |F_n(x) - F_S(x)| > \epsilon/R\right) \quad (28)$$

$$\leq 2 \exp(-Ck^2\epsilon^2/R^2) \quad (29)$$

$$\leq C_{p,R} \exp(k^2\epsilon^2), \quad (30)$$

for a constant $C_R > 0$, which completes the proof.

A.2 Proof of Proposition 2

We denote \mathcal{S} as the quantile sketch with initial size $k > 1$ constructed from streaming samples x_1, \dots, x_n from $\mu \in \mathcal{P}(\mathbb{R})$. Let define $F_n(y) = \frac{1}{n} \sum_{i=1}^n I(x_i \leq y)$, $F_{S,h}(y) = \frac{1}{n} \sum_{h=1}^{h'} \sum_{x \in C_h} w_h I(x \leq y)$, $F_n^{-1}(q) = \inf\{x : F_n(x) \geq q\}$, and $F_{S_\mu}^{-1}(q) = \inf\{x : F_{S_\mu}(x) \geq q\}$. For any $q \in [0, 1]$, we have:

$$\begin{aligned} \mathbb{P}(F_S^{-1}(q) > F_n^{-1}(q) + \epsilon) &= \mathbb{P}(F_S(F_n^{-1}(q) + \epsilon) < q) \\ &= \mathbb{P}(F_S(F_n^{-1}(q) + \epsilon) - F_n(F_n^{-1}(q) + \epsilon) < q - F_n(F_n^{-1}(q) + \epsilon)) \end{aligned} \quad (31)$$

From Appendix A.1, we know that $F_S(F_n^{-1}(q) + \epsilon) - F_n(F_n^{-1}(q) + \epsilon)$ is the sum of Bernoulli random variables, by the Hoeffding's inequality, we have:

$$\mathbb{P}(F_S^{-1}(q) > F_n^{-1}(q) + \epsilon) \leq \exp(-Ck^2(F_n(F_n^{-1}(q) + \epsilon) - q)^2), \quad (32)$$

for a constant $C > 0$. Similarly, we have:

$$\begin{aligned} \mathbb{P}(F_S^{-1}(q) \leq F_n^{-1}(q) - \epsilon) &= \mathbb{P}(F_S(F_n^{-1}(q) - \epsilon) \geq q) \\ &= \mathbb{P}(F_S(F_n^{-1}(q) - \epsilon) - F_n(F_n^{-1}(q) - \epsilon) \geq q - F_n(F_n^{-1}(q) - \epsilon)) \\ &\leq \exp(-Ck^2(q - F_n(F_n^{-1}(q) - \epsilon))^2). \end{aligned} \quad (33)$$

By the union bound, we have:

$$\begin{aligned} \mathbb{P}(|F_S^{-1}(q) - F_n^{-1}(q)| > \epsilon) &\leq \mathbb{P}(F_S^{-1}(q) - F_n^{-1}(q) > \epsilon) + \mathbb{P}(F_S^{-1}(q) - F_n^{-1}(q) \leq -\epsilon) \\ &\leq \exp(-Ck^2(F_n(F_n^{-1}(q) + \epsilon) - q)^2) + \exp(-Ck^2(q - F_n(F_n^{-1}(q) - \epsilon))^2) \\ &\leq 2 \exp(-Ck^2\gamma_{q,\epsilon}^2), \end{aligned} \quad (34)$$

where $\gamma_{q,\epsilon} = \min\{q - F_n(F_n^{-1}(q) - \epsilon), F_n(F_n^{-1}(q) + \epsilon) - q\}$.

Compact support. When having compact support (at most R), we have:

$$\begin{aligned} \mathbb{P}\left(\int_0^1 |F_S^{-1}(q) - F_n^{-1}(q)| dq > \epsilon\right) \\ = \mathbb{P}\left(\int_{\mathbb{R}} |F_S(x) - F_n(x)| dx > \epsilon\right) \leq 2 \exp(-Ck^2\epsilon^2/R^2), \end{aligned} \quad (35)$$

where the last inequality is proven in Appendix A.1.

A.3 Proof of Proposition 3

In one dimension, the p -Wasserstein distance admits the quantile representation

$$W_p^p(\mu_n, \nu_m) = \int_0^1 |F_{\mu_n}^{-1}(q) - F_{\nu_m}^{-1}(q)|^p dq, \quad (36)$$

and similarly

$$\widetilde{W}_p^p(\mu_n, \nu_m; \mathcal{S}_{\mu_n, k_1}, \mathcal{S}_{\nu_m, k_2}) = \int_0^1 |F_{\mathcal{S}_{\mu_n, k_1}}^{-1}(q) - F_{\mathcal{S}_{\nu_m, k_2}}^{-1}(q)|^p dq. \quad (37)$$

We have

$$\begin{aligned} & \left| \widetilde{W}_p^p(\mu_n, \nu_m; \mathcal{S}_{\mu_n, k_1}, \mathcal{S}_{\nu_m, k_2}) - W_p^p(\mu_n, \nu_m) \right| \\ &= \left| \int_0^1 |F_{\mathcal{S}_{\mu_n, k_1}}^{-1}(q) - F_{\mathcal{S}_{\nu_m, k_2}}^{-1}(q)|^p dq - \int_0^1 |F_{\mu_n}^{-1}(q) - F_{\nu_m}^{-1}(q)|^p dq \right| \end{aligned} \quad (38)$$

$$= \left| \int_0^1 \left(|F_{\mathcal{S}_{\mu_n, k_1}}^{-1}(q) - F_{\mathcal{S}_{\nu_m, k_2}}^{-1}(q)|^p - |F_{\mu_n}^{-1}(q) - F_{\nu_m}^{-1}(q)|^p \right) dq \right|. \quad (39)$$

For $a = |F_{\mathcal{S}_{\mu_n, k_1}}^{-1}(q) - F_{\mathcal{S}_{\nu_m, k_2}}^{-1}(q)|$, $b = |F_{\mu_n}^{-1}(q) - F_{\nu_m}^{-1}(q)|$, using the inequality:

$$a^p - b^p \leq p \max\{a, b\}^{p-1} (a - b), \quad (40)$$

and the following inequality (by the triangle inequality):

$$\begin{aligned} & \left| |F_{\mathcal{S}_{\mu_n, k_1}}^{-1}(q) - F_{\mathcal{S}_{\nu_m, k_2}}^{-1}(q)| - |F_{\mu_n}^{-1}(q) - F_{\nu_m}^{-1}(q)| \right| \\ & \leq |F_{\mathcal{S}_{\mu_n, k_1}}^{-1}(q) - F_{\mu_n}^{-1}(q)| + |F_{\mathcal{S}_{\nu_m, k_2}}^{-1}(q) - F_{\nu_m}^{-1}(q)| \end{aligned} \quad (41)$$

we obtain

$$\begin{aligned} & \left| \widetilde{W}_p^p(\mu_n, \nu_m; \mathcal{S}_{\mu_n, k_1}, \mathcal{S}_{\nu_m, k_2}) - W_p^p(\mu_n, \nu_m) \right| \\ & \leq p \int_0^1 \max \left\{ |F_{\mathcal{S}_{\mu_n, k_1}}^{-1}(q) - F_{\mathcal{S}_{\nu_m, k_2}}^{-1}(q)|^{p-1}, |F_{\mu_n}^{-1}(q) - F_{\nu_m}^{-1}(q)| \right\}^{p-1} \\ & \quad \left(|F_{\mathcal{S}_{\mu_n, k_1}}^{-1}(q) - F_{\mu_n}^{-1}(q)| + |F_{\mathcal{S}_{\nu_m, k_2}}^{-1}(q) - F_{\nu_m}^{-1}(q)| \right) dq. \end{aligned} \quad (42)$$

Since both measures are supported on an interval of diameter R , we have

$$\max \left\{ |F_{\mathcal{S}_{\mu_n, k_1}}^{-1}(q) - F_{\mathcal{S}_{\nu_m, k_2}}^{-1}(q)|^{p-1}, |F_{\mu_n}^{-1}(q) - F_{\nu_m}^{-1}(q)| \right\}^{p-1} \leq R^{p-1}$$

for all $q \in [0, 1]$, which yields

$$\begin{aligned} & \left| \widetilde{W}_p^p(\mu_n, \nu_m; \mathcal{S}_{\mu_n, k_1}, \mathcal{S}_{\nu_m, k_2}) - W_p^p(\mu_n, \nu_m) \right| \\ & \leq p \int_0^1 R^{p-1} \left(|F_{\mathcal{S}_{\mu_n, k_1}}^{-1}(q) - F_{\mu_n}^{-1}(q)| + |F_{\mathcal{S}_{\nu_m, k_2}}^{-1}(q) - F_{\nu_m}^{-1}(q)| \right) dq. \end{aligned} \quad (43)$$

Let $\delta = \epsilon/(2pR^{p-1})$. If $|\widetilde{W}_p^p(\mu_n, \nu_m; \mathcal{S}_{\mu_n, k_1}, \mathcal{S}_{\nu_m, k_2}) - W_p^p(\mu_n, \nu_m)| > \epsilon$, then at least one of the two integrals above exceeds δ . By Proposition 2 and a union bound,

$$\begin{aligned} & \mathbb{P}\left(|\widetilde{W}_p^p - W_p^p| > \epsilon\right) \\ & \leq \mathbb{P}\left(\int_0^1 |F_{S_{\mu_n, k_1}}^{-1}(q) - F_{\mu_n}^{-1}(q)| dq > \delta\right) + \mathbb{P}\left(\int_0^1 |F_{S_{\nu_m, k_2}}^{-1}(q) - F_{\nu_m}^{-1}(q)| dq > \delta\right) \\ & \leq 2 \exp(-C_R k_1^2 \delta^2) + 2 \exp(-C_R k_2^2 \delta^2) \leq 4 \exp(-C_R \min\{k_1, k_2\}^2 \delta^2). \end{aligned} \quad (44)$$

Substituting δ completes the proof with $C_{p,R} = C_R/(4p^2 R^{2(p-1)})$.

Population approximation. We begin with a decomposition of the error using the triangle inequality:

$$\begin{aligned} & \left| \widetilde{W}_p^p(\mu_n, \nu_m; \mathcal{S}_{\mu_n, k_1}, \mathcal{S}_{\nu_m, k_2}) - W_p^p(\mu, \nu) \right| \\ & \leq \left| \widetilde{W}_p^p(\mu_n, \nu_m; \mathcal{S}_{\mu_n, k_1}, \mathcal{S}_{\nu_m, k_2}) - W_p^p(\mu_n, \nu_m) \right| + \left| W_p^p(\mu_n, \nu_m) - W_p^p(\mu, \nu) \right|. \end{aligned} \quad (45)$$

Define the two terms

$$A := \left| \widetilde{W}_p^p(\mu_n, \nu_m; \mathcal{S}_{\mu_n, k_1}, \mathcal{S}_{\nu_m, k_2}) - W_p^p(\mu_n, \nu_m) \right|, \quad (46)$$

$$B := \left| W_p^p(\mu_n, \nu_m) - W_p^p(\mu, \nu) \right|. \quad (47)$$

Then for any $\epsilon > 0$, using the union bound:

$$\mathbb{P}(A + B > \epsilon) \leq \mathbb{P}(A > \frac{\epsilon}{2}) + \mathbb{P}(B > \frac{\epsilon}{2}), \quad (48)$$

From Proposition 3 yields

$$\mathbb{P}(A > \frac{\epsilon}{2}) \leq 4 \exp(-C_{p,R} \min\{k_1^2, k_2^2\} \epsilon^2/4). \quad (49)$$

For controlling of the statistical error B , by Lemma 4 in [19], there exists a constant $C'_{p,R} > 0$ such that

$$B \leq C'_{p,R} (W_1(\mu_n, \mu) + W_1(\nu_m, \nu)). \quad (50)$$

Hence,

$$\mathbb{P}(B > \frac{\epsilon}{2}) \leq \mathbb{P}(C'_{p,R} (W_1(\mu_n, \mu) + W_1(\nu_m, \nu)) > \frac{\epsilon}{2}) \quad (51)$$

$$\leq \mathbb{P}\left(W_1(\mu_n, \mu) > \frac{\epsilon}{4C'_{p,R}}\right) + \mathbb{P}\left(W_1(\nu_m, \nu) > \frac{\epsilon}{4C'_{p,R}}\right), \quad (52)$$

using the union bound once more.

By the Dvoretzky–Kiefer–Wolfowitz inequality and the compact support assumption,

$$\mathbb{P}(W_1(\mu_n, \mu) > \delta) \leq 2 \exp(-2n\delta^2/R^2), \quad (53)$$

and similarly for ν_m . Setting $\delta = \epsilon/(4C'_{p,R})$ gives

$$\mathbb{P}(B > \frac{\epsilon}{2}) \leq 4 \exp\left(-\frac{\min\{n, m\}\epsilon^2}{8R^2 C'^2_{p,R}}\right). \quad (54)$$

Substituting the bounds from Steps 1 and 2 into equation 48 yields

$$\mathbb{P}\left(\left|\widetilde{W}_p^p(\mu_n, \nu_m; \mathcal{S}_{\mu_n, k_1}, \mathcal{S}_{\nu_m, k_2}) - W_p^p(\mu, \nu)\right| > \epsilon\right) \leq 4e^{-a} + 4e^{-b}, \quad (55)$$

where

$$a = C_R \epsilon^2 \min\{k_1^2, k_2^2\}, \quad b = \frac{\min\{n, m\}\epsilon^2}{8R^2 C'^2_{p,R}}.$$

Using the inequality $e^{-a} + e^{-b} \leq 2e^{-\min\{a, b\}}$, we conclude that

$$\mathbb{P}\left(\left|\widetilde{W}_p^p(\mu_n, \nu_m; \mathcal{S}_{\mu_n, k_1}, \mathcal{S}_{\nu_m, k_2}) - W_p^p(\mu, \nu)\right| > \epsilon\right) \leq 8 \exp(-c_{p,R} \epsilon^2 \min\{k_1^2, k_2^2, n, m\}), \quad (56)$$

for a constant $c_{p,R} > 0$ depending only on p and R .

A.4 Proof of Proposition 4

For any $x \in \mathbb{R}$, use the natural triangle inequality decomposition:

$$\begin{aligned} |\widetilde{T}(x) - T_{\mu \rightarrow \nu}(x)| &= |F_{S_{\nu_m, k_2}}^{-1}(F_{S_{\mu_n, k_1}}(x)) - F_{\nu}^{-1}(F_{\mu}(x))| \\ &\leq |F_{\nu}^{-1}(F_{S_{\mu_n, k_1}}(x)) - F_{\nu}^{-1}(F_{\mu}(x))| + |F_{S_{\nu_m, k_2}}^{-1}(F_{S_{\mu_n, k_1}}(x)) - F_{\nu}^{-1}(F_{S_{\mu_n, k_1}}(x))|. \end{aligned} \quad (57)$$

Define the two terms

$$A := |F_{\nu}^{-1}(F_{S_{\mu_n, k_1}}(x)) - F_{\nu}^{-1}(F_{\mu}(x))|, \quad (58)$$

$$B := |F_{S_{\nu_m, k_2}}^{-1}(F_{S_{\mu_n, k_1}}(x)) - F_{\nu}^{-1}(F_{S_{\mu_n, k_1}}(x))|. \quad (59)$$

Since $f_{\nu} \geq m > 0$, the true quantile function F_{ν}^{-1} is $1/m$ -Lipschitz:

$$|F_{\nu}^{-1}(u) - F_{\nu}^{-1}(v)| \leq \frac{1}{m}|u - v|, \quad \forall u, v \in [0, 1].$$

Hence,

$$A \leq \frac{1}{m}|F_{S_{\mu_n, k_1}}(x) - F_{\mu}(x)|.$$

We further have:

$$\begin{aligned} \int_{\mathbb{R}} A d\mu(x) &\leq \frac{1}{m} \int_{\mathbb{R}} |F_{S_{\mu_n, k_1}}(x) - F_{\mu}(x)| d\mu(x) \leq \frac{1}{m} \sup_x |F_{S_{\mu_n, k_1}}(x) - F_{\mu}(x)| \\ &\leq \frac{1}{m} \sup_x |F_{S_{\mu_n, k_1}}(x) - F_{\mu_n}(x)| + \frac{1}{m} \sup_x |F_{\mu_n}(x) - F_{\mu}(x)| \end{aligned} \quad (60)$$

By Proposition 1 (integrated bound for quantile sketches), the Dvoretzky–Kiefer–Wolfowitz inequality, and the union bound:

$$\mathbb{P}\left(\int_{\mathbb{R}} A d\mu(x) > \frac{\epsilon}{2}\right) \leq 4 \exp(-C_m k_1^2 \epsilon^2), \quad (61)$$

for a constant $C_m > 0$. Similarly:

$$\int_{\mathbb{R}} B d\mu(x) \leq \sup_{q \in [0,1]} |F_{S_{\nu_m, k_2}}^{-1}(q) - F_{\nu_m}^{-1}(q)| + \int_0^1 |F_{\nu_m}^{-1}(q) - F_{\nu}^{-1}(q)| dq \quad (62)$$

$$= \sup_{q \in [0,1]} |F_{S_{\nu_m, k_2}}^{-1}(q) - F_{\nu_m}^{-1}(q)| + R \sup_x \int_{\mathbb{R}} |F_{\nu_m}(x) - F_{\nu}(x)| \quad (63)$$

Using Proposition 2, the Dvoretzky–Kiefer–Wolfowitz inequality, and the union bound:

$$\mathbb{P}\left(\int_{\mathbb{R}} B d\mu(x) > \frac{\epsilon}{2}\right) \leq 4 \exp(-C_R k_2^2 \epsilon^2). \quad (64)$$

By the union bound:

$$\mathbb{P}\left(\int_{\mathbb{R}} |\tilde{T}(x) - T_{\mu \rightarrow \nu}(x)| d\mu(x) > \epsilon\right) \leq \mathbb{P}\left(\int A > \epsilon/2\right) + \mathbb{P}\left(\int B > \epsilon/2\right) \leq 8 \exp\left(-c_{m,R} \epsilon^2 \min\{k_1^2, k_2^2\}\right), \quad (65)$$

for a constant $c_{m,R} > 0$ depending only on m and R .

A.5 Proof of Corollary 1

By definition of the sliced Wasserstein distance,

$$SW_p^p(\mu_n, \nu_m) = \mathbb{E}_{\theta \sim \sigma} \left[W_p^p(\theta_{\#} \mu_n, \theta_{\#} \nu_m) \right], \quad (66)$$

and similarly,

$$\widetilde{SW}_p^p(\mu_n, \nu_m; k_1, k_2) = \mathbb{E}_{\theta \sim \sigma} \left[\widetilde{W}_p^p(\theta_{\#} \mu_n, \theta_{\#} \nu_m; S_{\theta_{\#} \mu_n, k_1}, S_{\theta_{\#} \nu_m, k_2}) \right]. \quad (67)$$

Therefore, by the Jensen's inequality,

$$\begin{aligned} & \left| \widetilde{SW}_p^p(\mu_n, \nu_m; k_1, k_2) - SW_p^p(\mu_n, \nu_m) \right| \\ & \leq \mathbb{E}_{\theta \sim \sigma} \left[\left| \widetilde{W}_p^p(\theta_{\#} \mu_n, \theta_{\#} \nu_m; S_{\theta_{\#} \mu_n, k_1}, S_{\theta_{\#} \nu_m, k_2}) - W_p^p(\theta_{\#} \mu_n, \theta_{\#} \nu_m) \right| \right] \end{aligned} \quad (68)$$

Thus, Proposition 3 applies with Fubini's theorem, yielding

$$\mathbb{P}\left(\mathbb{E}_{\theta \sim \sigma} \left[\left| \widetilde{W}_p^p(\theta_{\#} \mu_n, \theta_{\#} \nu_m; S_{\theta_{\#} \mu_n, k_1}, S_{\theta_{\#} \nu_m, k_2}) - W_p^p(\theta_{\#} \mu_n, \theta_{\#} \nu_m) \right| \right] > \epsilon\right) \leq 4 \exp(-C_{p,R} \min\{k_1^2, k_2^2\} \epsilon^2), \quad (69)$$

which implies

$$\mathbb{P}\left(\left|\widetilde{SW}_p^p(\mu_n, \nu_m; k_1, k_2) - SW_p^p(\mu_n, \nu_m)\right| > \epsilon\right) \leq 4 \exp(-C_{p,R} \min\{k_1^2, k_2^2\} \epsilon^2). \quad (70)$$

Population approximation. By definition of the sliced Wasserstein distance, we have

$$SW_p^p(\mu, \nu) = \mathbb{E}_{\theta \sim \sigma} \left[W_p^p(\theta \# \mu, \theta \# \nu) \right]. \quad (71)$$

By the Jensen's inequality, we have

$$\begin{aligned} & \left| \widetilde{SW}_p^p(\mu_n, \nu_m; k_1, k_2) - SW_p^p(\mu, \nu) \right| \\ & \leq \mathbb{E}_{\theta \sim \sigma} \left[\left| \widetilde{W}_p^p(\theta \# \mu_n, \theta \# \nu_m; S_{\theta \# \mu_n, k_1}, S_{\theta \# \nu_m, k_2}) - W_p^p(\theta \# \mu, \theta \# \nu) \right| \right] \end{aligned} \quad (72)$$

Thus, Proposition 3 applies with Fubini's theorem, yielding

$$\mathbb{P}\left(\mathbb{E}_{\theta \sim \sigma} \left[\left| \widetilde{W}_p^p(\theta \# \mu_n, \theta \# \nu_m; S_{\theta \# \mu_n, k_1}, S_{\theta \# \nu_m, k_2}) - W_p^p(\theta \# \mu, \theta \# \nu) \right| \right] > \epsilon\right) \leq 8 \exp(-C_{p,R} \min\{k_1^2, k_2^2, n, m\} \epsilon^2), \quad (73)$$

which implies

$$\mathbb{P}\left(\left|\widetilde{SW}_p^p(\mu_n, \nu_m; k_1, k_2) - SW_p^p(\mu, \nu)\right| > \epsilon\right) \leq 8 \exp(-C_{p,R} \min\{k_1^2, k_2^2, n, m\} \epsilon^2), \quad (74)$$

which completes the proof.

A.6 Proof of Theorem 1

Let $\theta_1, \dots, \theta_L$ be i.i.d. random directions sampled uniformly from the unit sphere \mathbb{S}^{d-1} . We recall the MC estimation of Stream-SW:

$$\widehat{SW}_p^p(\mu_n, \nu_m; k_1, k_2, L) = \frac{1}{L} \sum_{l=1}^L \widetilde{W}_p^p(\theta_l \# \mu_n, \theta_l \# \nu_m; S_{\theta_l \# \mu_n, k_1}, S_{\theta_l \# \nu_m, k_2}). \quad (75)$$

By the triangle inequality:

$$\begin{aligned} & \left| \widehat{SW}_p^p(\mu_n, \nu_m; k_1, k_2, L) - SW_p^p(\mu, \nu) \right| \\ & \leq \left| \widehat{SW}_p^p(\mu_n, \nu_m; k_1, k_2, L) - \widetilde{SW}_p^p(\mu_n, \nu_m; k_1, k_2) \right| + \left| \widetilde{SW}_p^p(\mu_n, \nu_m; k_1, k_2) - SW_p^p(\mu, \nu) \right|. \end{aligned} \quad (76)$$

First, we have:

$$\begin{aligned} & \left| \widehat{SW}_p^p(\mu_n, \nu_m; k_1, k_2, L) - SW_p^p(\mu, \nu) \right| \\ & = \left| \frac{1}{L} \sum_{l=1}^L \left(\widetilde{W}_p^p(\theta_l \# \mu_n, \theta_l \# \nu_m; S_{\theta_l \# \mu_n, k_1}, S_{\theta_l \# \nu_m, k_2}) - \mathbb{E}_{\theta \sim \sigma} \left[\widetilde{W}_p^p(\theta \# \mu_n, \theta \# \nu_m; S_{\theta \# \mu_n, k_1}, S_{\theta \# \nu_m, k_2}) \right] \right) \right| \end{aligned} \quad (77)$$

due to the Jensen's inequality.

Since we assume having compact support, we have $0 \leq \widetilde{W}_p^p(\theta_l \# \mu_n, \theta_l \# \nu_m; S_{\theta_l \# \mu_n, k_1}, S_{\theta_l \# \nu_m, k_2}) \leq R^p$ for any $\theta \in \mathbb{S}^{d-1}$. Therefore,

$$0 \leq \widetilde{W}_p^p(\theta_l \# \mu_n, \theta_l \# \nu_m; S_{\theta_l \# \mu_n, k_1}, S_{\theta_l \# \nu_m, k_2}) - \mathbb{E}_{\theta \sim \sigma} \left[\widetilde{W}_p^p(\theta \# \mu_n, \theta \# \nu_m; S_{\theta \# \mu_n, k_1}, S_{\theta \# \nu_m, k_2}) \right] \leq R^p, \quad (78)$$

for any $\theta \in \mathbb{S}^{d-1}$. Using the Hoeffding's inequality:

$$\begin{aligned} & \mathbb{P} \left(\left| \frac{1}{L} \sum_{l=1}^L \left(\widetilde{W}_p^p(\theta_l \# \mu_n, \theta_l \# \nu_m; S_{\theta_l \# \mu_n, k_1}, S_{\theta_l \# \nu_m, k_2}) - \mathbb{E}_{\theta \sim \sigma} \left[\widetilde{W}_p^p(\theta \# \mu_n, \theta \# \nu_m; S_{\theta \# \mu_n, k_1}, S_{\theta \# \nu_m, k_2}) \right] \right) \right| > \epsilon/2 \right) \\ & \leq 2 \exp \left(-\frac{0.5L\epsilon^2}{R^{2p}} \right). \end{aligned} \quad (79)$$

From Corollary 1, we further have:

$$\mathbb{P} \left(\left| \widetilde{SW}_p^p(\mu_n, \nu_m; k_1, k_2) - SW_p^p(\mu, \nu) \right| > \epsilon/2 \right) \leq 8 \exp(-C_{p,R}/4 \min\{k_1^2, k_2^2, n, m\} \epsilon^2). \quad (80)$$

Using the union bound:

$$\mathbb{P} \left(\left| \widetilde{\widetilde{SW}}_p^p(\mu_n, \nu_m; k_1, k_2, L) - SW_p^p(\mu, \nu) \right| > \epsilon \right) \leq 10 \exp(-c'_{p,R} \min\{k_1^2, k_2^2, n, m, L\} \epsilon^2), \quad (81)$$

where $c'_{p,R} > 0$ is a constant depending only on p and R . We complete the proof.

B Additional Materials

One-sided Stream-SW. We first state the one-sided version of streaming 1DW and Stream-SW.

Definition 3. Given two empirical distributions μ_n and ν_m observed in a streaming fashion, and the corresponding quantile sketch \mathcal{S}_{μ_n, k_1} of μ_n $k_1 > 1$, one-sided streaming one-dimensional Wasserstein is defined as follow:

$$\widetilde{W}_p^p(\mu_n, \nu_m; \mathcal{S}_{\mu_n, k_1}, \mathcal{S}_{\nu_m, k_2}) = \int_0^1 \left| F_{\mathcal{S}_{\mu_n, k_1}}^{-1}(q) - F_{\mathcal{S}_{\nu_m, k_2}}^{-1}(q) \right|^p dq. \quad (82)$$

Definition 4. Let $k_1 > 1$, and $p \geq 1$. The one-sided streaming Sliced Wasserstein (Stream-SW) distance between two empirical distributions $\mu_n \in \mathcal{P}_p(\mathbb{R}^d)$ and $\nu_m \in \mathcal{P}_p(\mathbb{R}^d)$, whose supports are observed in a streaming manner, is defined by

$$\widetilde{SW}_p^p(\mu_n, \nu_m; k_1) = \mathbb{E}_{\theta \sim \sigma} \left[\widetilde{W}_p^p(\theta \# \mu_n, \theta \# \nu_m; S_{\theta \# \mu_n, k_1},) \right], \quad (83)$$

where $\sigma \in \mathcal{P}(\mathbb{S}^{d-1})$ is a slicing distribution on the unit sphere and $\widetilde{W}_p^p(\theta \# \mu_n, \theta \# \nu_m; S_{\theta \# \mu_n, k_1},)$ is defined in Definition 3.

Gradient approximation. When using SW as an empirical risk for minimization with respect to a parametric distribution, e.g., μ_ϕ , we might be interested in computing the gradient $\nabla_\phi SW_p^p(\mu_\phi, \nu)$ e.g., in point cloud applications and generative modeling applications. We can

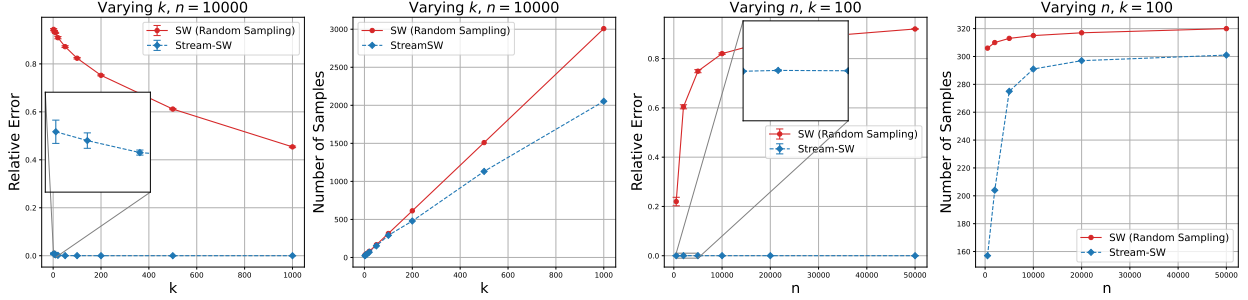


Figure 5: Relative errors and number of samples when comparing Gaussian distributions

rewrite $\nabla_{\phi} \text{SW}_p^p(\mu_{\phi}, \nu) = \nabla_{\phi} \mathbb{E}_{\theta \sim \sigma(\theta)} \left[\int_{\infty}^{\infty} |\theta^{\top} x - F_{\theta_{\#}^{-1}}^{-1}(F_{\mu_{\phi}}(x))|^p d\mu_{\phi}(x) \right]$. When μ_{ϕ} is reparameterizable i.e., $\mu_{\phi} = f_{\phi} \# \epsilon$ with ϵ is a random noise distribution, we can rewrite $\text{SW}_p^p(\mu_{\phi}, \nu) = \mathbb{E}_{\theta \sim \sigma(\theta)} \left[\int_{\infty}^{\infty} \nabla_{\phi} |\theta^{\top} x - F_{\theta_{\#}^{-1}}^{-1}(F_{\mu_{\phi}}(f_{\phi}(z)))|^p d\epsilon(z) \right]$. By using Monte Carlo estimation to approximate expectation and integration, and using streaming approximation for quantile functions (and CDFs), we can form a stochastic estimation of the gradient with respect to ϕ .

C Additional Experiments

Gaussian Comparison. We simulate samples from the following two Gaussians $\mathcal{N}((-1, -1), I)$ and $\mathcal{N}((2, 2), I)$. We investigate the approximation error and the number of samples keeping from the stream when increasing k (sketch size) and n (number of supports). We set the number of projections $L = 1000$, we vary $k \in \{2, 5, 10, 20, 50, 100, 200, 500, 1000\}$ when keeping $n = 1000$, and vary $n \in \{500, 2000, 5000, 10000, 20000, 50000\}$ when keep $k = 100$. We show the relative approximation error (absolute difference of the estimated distance from the true distance divided by the true distance) with 10 different runs in Figure 5. Here, we compare Stream-SW with SW using random sampling to retain $3k + 2 \log(n/(2k/3))$ samples. From the figure, we see that Stream-SW can achieve significantly better relative error and requires fewer samples.

Gradient flows. As discussed, we visualize flows for $(L = 100, k = 100)$ in Figure 6, $(L = 100, k = 200)$ in Figure 7, and $(L = 1000, k = 100)$ in Figure 8. The qualitative comparison is consistent with the quantitative result in Table 1. We see that increasing k and increasing L leads to better gradient flows in both Wasserstein-2 and perceptual visualization.

Streaming change point detection. The conventional approach is to use a sliding window to detect sudden changes in the stream. However, the sliding window approach for change point detection has several limitations. Choosing an appropriate window size is difficult, as small windows may miss context while large ones can dilute localized anomalies. Anomalies near window boundaries may be partially captured or missed, and the method can be computationally expensive with small step sizes. It often ignores temporal dependencies across windows, introduces detection delays, and suffers from class imbalance due to sparse anomalies. Additionally, it lacks adaptability to changing patterns and may lose important context that spans multiple windows.

We follow a different approach where we compare the observed pre-detection distribution with the full observed distribution over time. It means that we decide that it is an anomaly when the distribution



Figure 6: Gradient flows from Full SW, SW with random sampling, and Stream-SW in turn ($L = 100, k = 100$).



Figure 7: Gradient flows from Full SW, SW with random sampling, and Stream-SW in turn ($L = 100, k = 200$).



Figure 8: Gradient flows from Full SW, SW with random sampling, and Stream-SW in turn ($L = 1000, k = 100$).

is changed significantly. Thank to the proposed Stream-SW, the distribution comparison can be

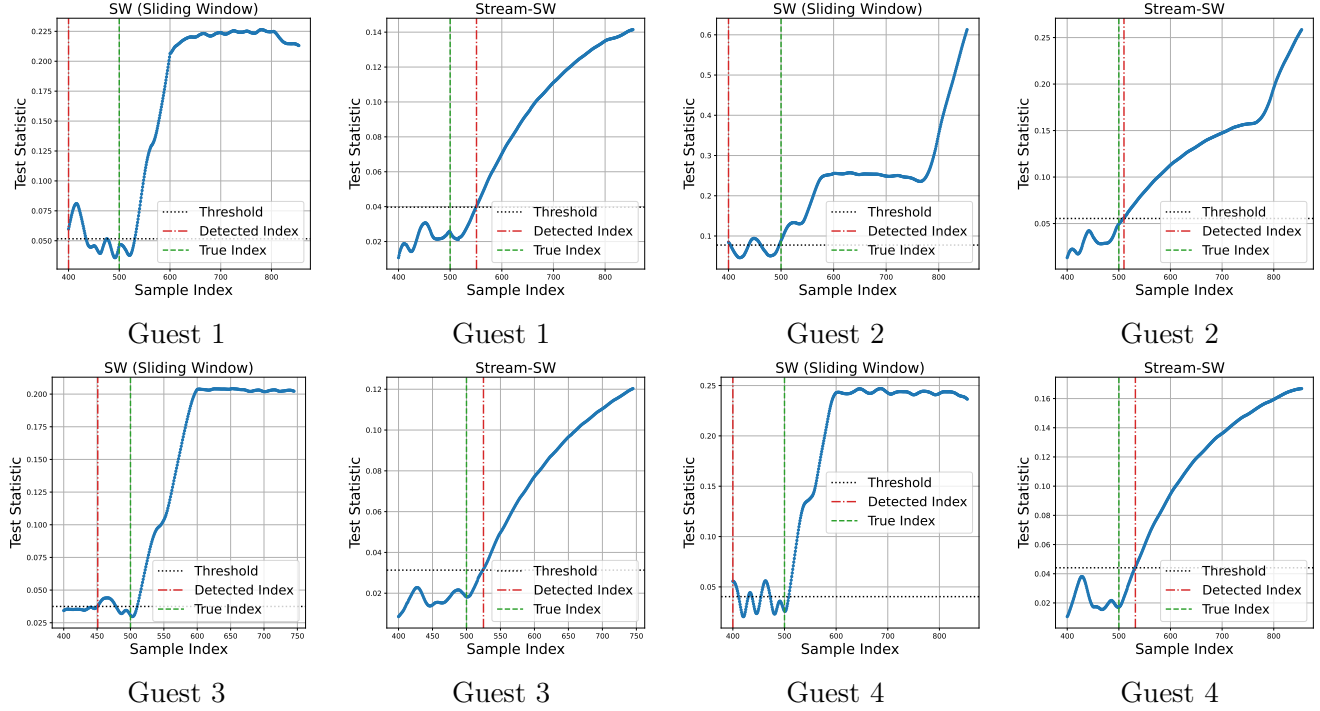


Figure 9: The figure shows the decision statistics, decision thresholds (null statistics), the true time index (where the change in action happens), and the detected indices, for both two approaches i.e., SW (Sliding window) and Stream-SW for the four guests.

conducted from the stream of samples.

As discussed in the main text, we use bootstrap to calculate the null statistic (decision threshold) from observed pre-detection data. We show the decision statistics, decision thresholds (null statistics), the true time index (where the change in action happens), and the detected indices, for both two approaches i.e., SW (Sliding window) and Stream-SW for the four guests in Figure 9. We observe that Stream-SW with the new detection approach leads to a more accurate detection. We would like to recall that we focus on comparing Stream-SW with SW only. The detection quality can be further improved by using other advanced kernel tricks, projection optimization techniques, and distributional projection operators [55, 14, 24].

D Computational Infrastructure

We use a HP Omen 25L desktop for conducting experiments.